Chapter 1

Introduction

Laser welding is a joining technology having broad scientific interest with advantages in diverse range of industries i-e aerospace, automotive, nuclear power plants, electronics and other industries. This technology, now a days, has widely been used and discussed in literature to explore new dimensions for welding of dissimilar materials such as welding of steel to titanium [1], steel-kovar, copper-aluminium and copper-steel [2] and magnesium alloy A5023-0 to AZ31B [3]. Although, the major objective behind joining of dissimilar materials is to take the advantage of each materials attributes i-e., thermal and electrical properties, corrosion resistance, tensile strength, Young's Modulus, Hardness and biocompatibility in order to intensify product performance or to inaugurate new functionalities [4]. However, it could be very difficult to weld different combinations of dissimilar materials owing to difference in physical, chemical and thermal properties such as discussed by Borrisutthekul et al. [3] for joining of magnesium/aluminum alloys. Moreover, in joining of SS-Ti, based on phase diagram Fe-Ti that solubility of Iron in Titanium is quite low owing to which intermetallic phases Fe-Ti and Fe_2Ti start to form which eventually leads to spontaneous breaking of joining materials [5]. Actually, the intermetallic phases are believed to be brittle due to thermal stress contradiction which need to be particularly subdue in order to have a reliable joint between dissimilar materials.

Several studies have reported different techniques to reduce intermetallic and strengthening of joining materials, with particular focus on steel and titanium, including diffusion bonding [6, 7], explosive welding [8, 9] and brazing [10, 11], arc welding, friction stir welding, ultrasonic welding and electron beam welding. All of these techniques, nevertheless minimize the

intermetallic between dissimilar materials to some degree but the practical application of these techniques are still restricted due to joint configuration, extensive intermetallic formation, transmit large stresses and vacuum problems. Recently, laser welding has shown to be an efficient technique for successful joining of stainless steel to titanium. Laser welding of titanium and stainless steel has been conducted by [12, 13] using Nd:YAG and CO_2 lasers with varying parameters along with use of different types of fillers in order to suppress the intermetallic. The results showed the satisfactory tensile strength of the welded sample.

Titanium alloys have high specific strength and corrosion resistance, due to which, these are being used widely in industrial applications and dental restorations [14]. Austenitic stainless steel due to its corrosion resistance is widely used in many industrial sectors including food processing, fertilizers, petrochemical, petroleum and nuclear power plants. Welding of austenitic stainless steel is widely used in industry due to component's manufacturing. As compared to ferritic steels, austenitic stainless steels have high internal stresses in welded parts and thermal distortion due to lower thermal conductivity and higher thermal coefficients of expansion which expand the openness of weld to hot cracks. Sensitization is another possible welding problem of austenitic stainless steel. Carbide precipitation is a major issue in welding austenitic stainless steel when done with gas tungsten arc welding but it can be minimized using laser welding.

Laser welding has a great advantage due to its high speed, quality, high cooling rate, excellent controllability, increased productivity that leads to reduce cost and ability to perform weld in non-vacuum environment. Laser butt welding of titanium Ti-6Al-4V and stainless steel 316L is performed by 2.5KW CO_2 Laser. Stainless steel 316L is extra low carbon version of 316. It is used because of minimizing harmful carbide precipitation during welding. Titanium Ti-6Al-4V is used as it's the widely used in industrial applications. To get full penetration of the weld, first

bead on plate is performed. After getting the required parameters of welding, autogenous welding is performed and then with filler material. Copper, Nickel and aluminum are used as filler material. Laser butt welding of titanium alloy to steel need copper as filler to enhance metallurgical reaction and minimize residual stresses [15]. Laser welding was done using Nd: YAG laser.

In present research, CO_2 laser is used instead of Nd:YAG laser for welding. Aluminium, nickel and copper is used as a filler to see whether it suppress intermetallics and what is the effect on the strength of the weld. Laser beam was positioned at an offset of 0.2mm on titanium. Microstructure and strength of the dissimilar material pair is investigated using Optical Microscope. Effect of varying laser scan speed on microstructure and penetration with respective to constant power is investigated as well. Tensile strength of the resulting welded specimen is determined.

Chapter 2

Literature Review

2.1 Laser Welding of Dissimilar Metals: Literature review

In the past few years laser welding has become an acceptable and reliable processing tool for the manufacturing industry. It has found applications in areas where conventional processes are not able to perform work because of heat input, vacuum, distortion and location. Commercial laser welding systems are available with a few watts of pulsed 1.06 μm wavelength radiation form CO_2 laser. These systems are capable of melting nearly all types of metals and alloys.

Since the development of high power CO_2 laser in the sixties, laser processing of materials has become a significantly important research filed. Lasers provide an intense heat source which is very useful for welding, cutting, cladding heat treatment etc. Each of these applications has now become a separate widespread research field. Hence in this part of literature survey, no attempt is made to review the whole field of laser processing, but only the important aspects of CO_2 lasers, laser material interaction mechanisms, and an in-depth review of papers concerning laser welding will be covered.

2.2 Fundamental of Lasers

The basic physics for producing laser light is the spontaneous emission and stimulated emission. All lasers work by exciting active medium which is place between two mirrors, one of which is partially transmitting Figure 2.1.

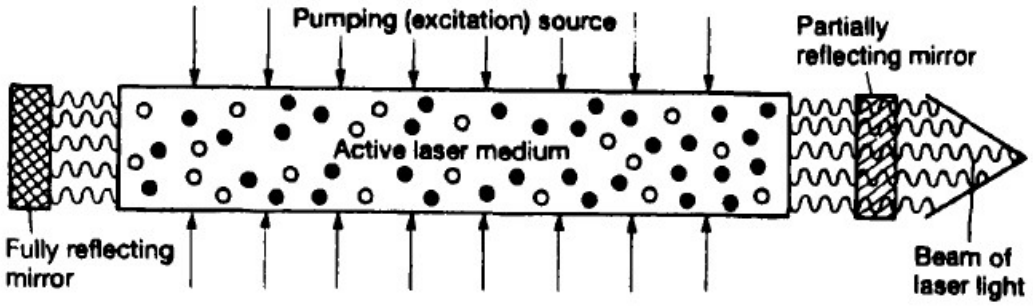

Figure 2.1. The basic element of Laser

There are three different ways in which radiation can interact with matter causing change in energy levels.

1. **Fluorescence**
2. **Absorption**
3. **Stimulated emission**

2.2.1 Fluorescence

Electron can be raised from lower to higher level in many ways. When this excited state is achieved, electron can decay to lower energy level in the absence of electromagnetic field, resulting in radiation energy.

2.2.2 Absorption

When electron lying in lower energy level interacts with the light, it results in raising the electron to higher energy level. Thus the electron absorbs the incident light.

2.2.3 Stimulated Emission

Stimulated emission is a transpose process of absorption. An electron in the higher energy level is stimulated by incoming radiation of frequency v, to release its energy and fall to a lower energy

level. In other words, a photon release a new photon rather than being absorbed. It has the same phase as that of first photon. The resulting photon has the tendency to produce two more photons which travel in the same direction and have same frequency as shown in Figure 2.2. By this process, large number of in phase photons can be obtained with the incident photons.

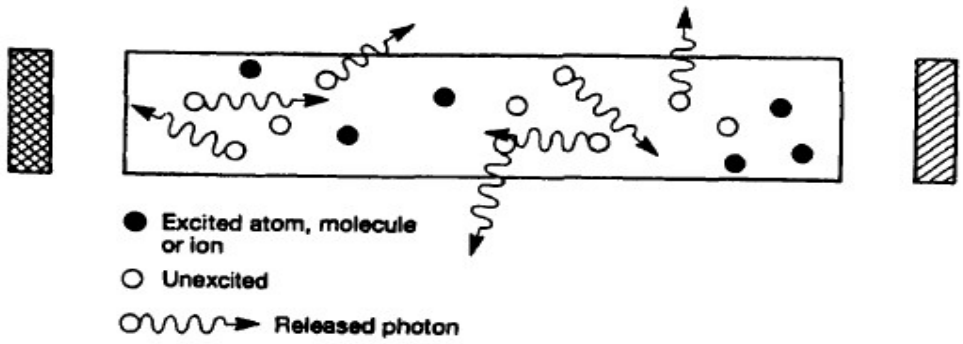

Figure 2.2. Emission of photons from excited active medium.

2.3 Properties of Lasers

Lasers have unique properties such as coherence and polarization.

2.3.1 Coherence

Coherence means different parts of electromagnetic waves that are in phase with one another. Coherence has two types. Temporal coherence and spatial coherence. Temporal coherence outline phase relation in direction of beam while spatial coherence outline phase relation perpendicular to the direction of propagation of beam.

2.3.2 Polarization

Laser light travel in the form of transverse waves of magnetic and electric vectors which are perpendicular to the propagation vector. Polarization describes orientation of magnetic and electric vectors of photons in a beam of radiation.

Plane or linear polarization is the simplest form in which electric field position is constant with time, only the sign and magnitude of field changes. The wave is said to be linearly polarized in y direction if the electric field is always pointing along the y-axis. Laser light is said to be unpolarized if plane of vibration are arbitrarily oriented about the direction of propagation. For circular polarized beams the electric vector is revolving.

2.4 Types of Lasers

Lasers can be made from solid, liquid and gases. The technique of excitation for lasing differs too; it can be by chemical reaction, light, electricity or using another laser. The lasers can be categorized as:

2.4.1 Solid State Lasers

2.4.2 Dye or Liquid Lasers and

2.4.3 Gas Lasers

2.4.1 Solid State Lasers

Solid state lasers are made from transparent materials like Yttrium Aluminum Garnet (YAG), emerald, synthetic ruby and Nd doped glass. Brilliant flash of light or focused intense light is used to excite these into lasing. These lasers are made from transparent crystal to let in the light. In industry the most common solid state lasers are Neodymium glass and Neodymium-Yttrium Aluminum Garnet.

2.4.2 Dye or Liquid Lasers

The construction of liquid laser is quite different than gas or solid state lasers. Liquid solutions of different dye materials are used. Dye materials are dissolved in organic solvents. Thus the active medium for dye laser is a liquid. Dye lasers are less common than solid state or gas lasers but

they possess certain unique advantages for certain application [16]. Gas lasers have smaller concentration of active lasing atoms because atoms are much further apart. In solid state lasers, thermal stresses are the major issue that can damage the active material but in liquid lasers, concentrations of active atoms are high. It is damage free and laser medium is cheap as well. One unique feature of dye lasers is that they can generate beams of varying tunable wavelength. This is due to the fact in a liquid excited atoms give a wide range of light. The laser has a prism to split this light into shrink wavelengths and the beam can be turned to varying wavelengths from Ultraviolet to infrared. The disadvantages are they operate at low power and are very inefficient.

2.4.3 Gas Lasers

Gas lasers are those in which gas is used as lasing medium. Gas lasers can be operated as pulsed or continuous. Three types of gas lasers are eminent depending upon the nature of lasing medium. Atomic, ionic and molecular. Electric discharge is normally employed for exciting the lasers into lasing.

2.5 Carbon Dioxide Lasers

Carbon dioxide laser is the most efficient gas laser and the most powerful continuously operating laser. It works in infrared region with a wavelength of 10.6μm [17]. CO_2 lasers are widely used in industry for drilling, cutting, welding and heat treatment.

CO_2 laser has three basic designs referred to as slow axial flow (SF), fast axial flow (FSF) and transverse flow (TF) as shown in figure. For axial flow lasers, the discharge, the flow of gas and the laser beam are co-axial while for transverse flow lasers, the discharge, the laser beam and the flow of gas are orthogonal to each other. Cooling is achieved by convection in TF and FSF while cooling in SF is achieved through cavity walls.

2.5.1 Principle of Operation

CO_2 laser operates by electric excitation of active medium. This active medium is a mixture of nitrogen, carbon dioxide and nitrogen. Total pressure of these gases is around 5kPa, permitting electrical energy to be coupled to the N_2 molecules in a stable glow discharge. It is most often done with high voltage direct current. The excited nitrogen shift energy to carbon dioxide molecules by through collision. The process is effective only if the CO_2 is cold, so energy level matches with the nitrogen. There are many energy levels of excited CO_2 that it can drop to around 9.6 and 10.6mm. The thermodynamic efficiency of system is around 30% [18]. Real CO_2 lasers seldom exceed 10% efficiency. So it is very important to main a low gas temperature in CO_2 lasers. For high power systems, heat exchangers are employed for keeping the gas cool.

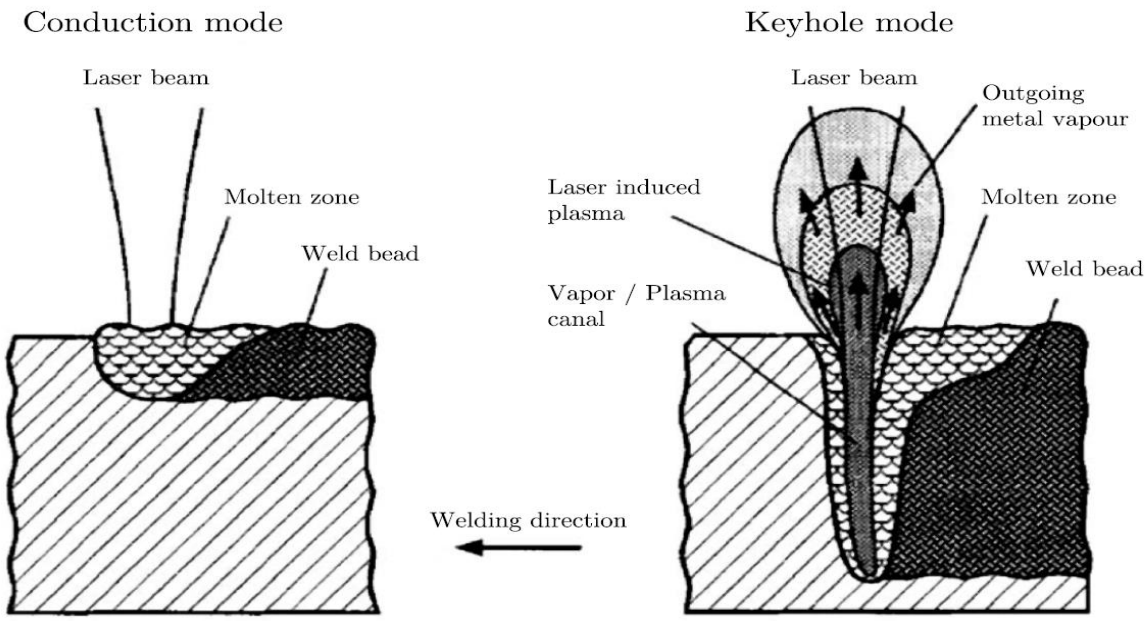

Figure 2.3: Cross view of the two different melting modes: (left) Conduction mode, (right) keyhole mode. The penetration depth is higher in keyhole mode as the absorption increases due to the formation of a plasma and the beam is focused down the canal by complete reflection on its wall.

2.6 Laser Parameters

2.6.1 Effect of Laser Power on Penetration

Laser power is the single most important factor affecting the welding process. It controls both the limit of penetration and the range of processing speeds. A Gaussian beam has a power intensity pattern with a peak in the center and a decline in intensity to the edges. The power intensity distribution, I, as a function of, r, from the center of a Gaussian beam is given by [19]

$$I(r) = I_0 \exp[-2r^2/r_0^2]$$

Where I_0 is the intensity of the beam at the center and r_0 is the Gaussian beam radius i.e. the radius at which the intensity has fallen to its central value by a factor of e^2, r is the radial position from the central Gaussian peak and I(r) is the laser beam intensity at radial point r.

The relationship between power and penetration has been studied by many workers. Baardsen et al. [20] and Lock at al. [21] showed a relationship between laser power and welding speed. They reported that penetration increases almost linearly with the increase in laser power. Willgoss et al. [22] showed a relationship between penetration and laser power using 7KW laser power for stainless steel 316. They found a linear relationship in the power range of 2.7 to 7KW, but below 2.5KW beam power welding without keyhole formation occurred, and hence a decrease in penetration was observed.

2.6.2 Effect of Beam Mode on Penetration

Mode structure is distribution of power across the beam. The beam mode structure can be represented in either symmetrical or cylindrical symmetry of TEM_{mn}. TEM_{00} is the lowest order

mode, referred to as the "Gaussian" mode. TEM_{10} mode is called "doughnut" mode. Factors affecting mode structure are the gain of cavity, pumping power, geometry of the laser cavity and optics and inhomogeneity in laser medium [23]. The effect of mode structure is reported by Sharp and Steen [24]. Sharp et al. showed that higher order mode decreases the penetration and increases the width of melted zone.

2.6.3 Effect of Wavelength

Wavelength has large effect on a working laser. Shorter wavelength gives higher absorption of the laser beam and less reflectivity while longer wavelength gives lower absorption and higher reflectivity to a variety of materials [25].

2.6.4 Effect of Spot Size on Weld Penetration

Spot size of laser beam decides the power intensity of beam. Ready [26] defines the unfocussed beam diameter as being the radius at which the power density has fallen to 1/e of the central value while Duley [19] defined it as the radius at which the intensity has fallen to $1/e^2$ of its central peak value. Ready [33] and Duley [7] have shown that a for a Gaussian beam the minimum spot size D_f is given by

$$D_f = {}^{2\lambda f}/_{\lambda D}$$

Where, f; focal length of the lens, λ: wavelength of the incident radiation, D; diameter of beam at lens. Thus the smaller the f/D ratio the smaller is the beam diameter. Therefore, when a higher power density is required, a low output of TEM_{00} mode may be more advantageous than a higher output power in higher order modes.

2.7 Characteristics of focusing optics

2.7.1 Focal Length

The focal length of the focusing optics play a vital role. The longer the focal length lens gives a longer depth of focus, but reduce penetration due to larger focal point. Ready [17], Seaman [27] and Engel [28] has shown that the use of a shorter focal length lens gives better penetration as it produces a smaller focal point and hence a higher power density on the surface of the metal.

2.7.2 Effect of Focal Position on Penetration

The location of the focal point position is critical to maintain adequate power density. Width and penetration of weld nugget can be controlled by the positioning of the focal point with respect to the surface of the joint. Maximum power is obtained at the focal point. Effect of focus on shape of fusion zone and on penetration depth is studied by several scientist [21, 26]. Optimum position of focus was found to be inside the material. Engel found the optimum position of focus for several metals (e.g. 1018 steel). Wilgoss et al. [22] studied the effect on weld profile, by moving the focal point 2.5mm distance each time towards the work piece. Alexander J. [29] used a 5.5KW laser and a welding speed of 40mm/s. She found that the maximum penetration is obtained with the focus of the beam 2mm below the surface of the work piece. Banas [30] and Eboo [31] found that the most effective penetration was achieved with focus at the surface. Seaman [27] suggested that the optimum position depends upon laser power.

2.8 Properties of Work piece

2.8.1 Reflectivity

Fraction of incident radiation absorbed for opaque solid is $\text{Ɛ} = 1\text{-}R_0$ where Ɛ is the emissivity and R_0 is the reflectivity at normal incidence. The reflectivity varies with the wavelength of laser radiation, the angle of incidence of the light on the surface, temperature of material and its polarization [25]. For laser processing of NaCl and Si, a wavelength between 1 and 10 μm is suitable and for iron and aluminum shorter wavelength are reliable.

As the laser light falls on the material, it heats up the surface and increases the absorptivity of the laser beam to the work piece [25] until the laser reaches a critical value I_c, the absorption rises to a higher value approaching unity and hence the laser processing efficiency increases considerably.

2.8.2 Effect of Welding Speed on Penetration

The second primary control over weld penetration is provided by welding speed. The welding speed, like power, determines under given conditions of welding the depth of penetration that can be achieved in the material. The relationship between traverse speed and penetration has been reported by many researchers [28, 32]. It is evident that increasing the welding speed decreases the penetration. Merchant [33] reported that insufficient penetration results if the welding speed is too fast and if the speed is too low, the molten material simply falls out of the keyhole before it resolidifies. At very low speed there is an increased interaction between laser beam and plasma which lessens the penetration [21].

2.8.3 Effect of Gas Shielding on Penetration

During a welding operation it is necessary to blanket the weld by a shielding gas to prevent the weld from oxidizing. Helium and argon are both inert gases commonly used in laser welding. Due to ionization of the shielding gas, plasma can be produced during laser welding. At high speeds this enhances the coupling and at low speed the plasma thickness interferes with the beam.

Seaman [34] and Herziger [35] investigated the effect of different shielding gases on penetration. They found that Helium gas gives better penetration than any other gas. This was due to higher ionization potential and consequently reduced absorption of radiation. On the other hand, argon increases the plasma which develops above the melting zone and also increase the absorption of energy, hence reduced penetration is obtained at low speeds. Seaman [34] reported that both the composition and flow rate of shielding gas influence the depth of penetration. Addition of 10% argon to helium in beneficial as it gives increased welding speeds while maintaining satisfactory blanketing.

A second function of the shielding as is focusing lens protection. The lens is close to the keyhole from which vapor and molten metal is ejected with considerable force. In laser powers up to 2kW a gas stream coaxial to the laser beam can stop this material form hitting the lens while protecting the weld.

2.9 Welding of Dissimilar Material Pairs

Need of dissimilar metals have increased from various perception such as cost saving, environmental concern, energy saving etc. It’s a challenging task these days to join dissimilar materials. The major problem in joining dissimilar material pair is formation of brittle intermetallic layers in the bond region, which results in low joining strength. Lots of efforts have

been made in order to achieve the bonding using fusion welding. Laser welding is extremely useful in controlling the formation of brittle intermetallics due to its high control in molten pool size and heat input.

Sun and Karppi [36] have study electron beam welding of dissimilar materials. They prominence on how to achieve dissimilar metal joints. As electron beam welding needs vacuum to perform welding, limitations are discussed but these difficulties are minor as compared to conventional arc welding. Review suggested that further research is to be needed to examine complications. Zhang Li and Fontana [37] investigated formation of butt joints between AISI304L and AISI12L13 using laser welding technique. They concluded to avoid solidification cracking in fusion zone, offset and angle of laser beam are key parameters for having a successful joint. The strength produced was higher than both the yield strength of AISI12L13 and AISI304L.

Diffusion bonding is another technique for joining dissimilar metals in which two metals are bonded in solid state. This enable to weld wide range of materials which are not able to be welded using conventional welding methods. Orhan [38] introduces a mathematical model to foretell the final bonding time. The model deduce a new creep mechanism for duplex alloys. Bejar [39]researched on similar and dissimilar couples steel bars SAE 5160, 1020 or 1045 using electro contact discharge forge welding. Tension tests were utilized for accessing the quality of welds. Bejar deduced all steel couples could be welded using this welding technique. Kahciar and Baylan [40] worked on dissimilar weld between X20CrMo13 grade martensitic stainless steel and X5CrNi18-10 grade austenitic and evaluated tensile strength, corrosion resistance, toughness and metallurgical characteristics. Defect free welds were made. Hardness was increased in both welds. Study suggested that austenitic stainless steel and martensitic stainless steel can be joined using both filler metals.

Satyanarayana [41] investigated continuous drive friction welding of austenitic and ferritic stainless steel. Major emphasize was on microstructure-mechanical property correlation and fracture reaction. Welding was successful but only on certain parameter combination. Joints were evaluated for resistance to pitting and concluded that dissimilar metal welds show lower resistance to pitting corrosion as compared to austenitic and ferritic stainless steel welds. Strength and toughness properties of dissimilar metal welds found to be better than ferritic stainless steel. Srinivasam [42]worked on dissimilar metal welding between carbon steel and duplex stainless steel. Shielded metal arc welding was used to weld CS to DSS with E309 and E2209 electrodes. Impact strength and hardness produced with E2209 electrode were better than E309. Corrosion resistance was found to be better when E309 electrode was used. Satyanarayana concluded that for joining CS to DSS, E2209 is most reliable consumable. Another technique for welding AISI 420 stainless steel to 304 stainless steel was investigated by Berretta [43] using pulsed Nd: YAG laser. Weld characteristics were investigated with the influence of laser beam position on joints. Offset of 0.1 to 0.2 mm towards 420 stainless steel and 304 stainless steel were made. The joints were investigated for pores, cracks and to predict the weld geometry. Mechanical properties were determined using Vickers micro hardness testing and tensile testing. SEM was used to determine the elements across the weld. Results suggested how to get the best weld regarding position of incident laser beam.

Luijendjk [44]carried out series of experiments on welding of dissimilar aluminum alloys using Gas Tungsten Arc Welding. Plate thickness of 1.5, 3 and 5mm were used. Skewness of weld and melting behavior of welding grooves were investigated. Strength of material in heat affected zone was weakened due to welding. For strain hardened and solution hardened alloys, reduction in strength was smaller but it was large for precipitation hardened alloys. Lee [45] investigated

dissimilar metal welding between aluminum alloys using friction stir welding. A356 Al alloy and wrought 6961 Al alloy were joint and evaluated using different welding speeds. Microstructure of joint showed assorted structures of materials. Onion ring pattern were observed in the stir zone. Microstructure of stir zone showed that it is composed of material that is fixed at the receded side. Dissimilar weld joints between Ti_3Al and TC4 were investigated by Zhang [46] using electron beam welding. Zhang investigated microstructure using TEM, XRD, SEM. Tensile testing was done to check the strength of the joint. Microstructure showed the structure to be martensite that appeared as coarse equiaxed grains. By increasing the heat input, there was no variation in the composition of weld but grain size increased significantly. Tensile strength obtained was near to Ti_3Al alloy. Micro hardness showed that hardness increased significantly in heat affected zone of both metals. The tensile strength of the joint was affected by grain size and grain size increases due to heat input. Abdollah-Zadeh [47] studied mechanical properties and microstructure of aluminum 1060 with copper (99.99%) in lap joint configuration using friction stir welding. Welding speed and rotational speed were adjusted to obtain best mechanical properties. Microstructure analysis showed that AlCu, Al_4Cu_9 and Al_2Cu were the intermetallics formed in the welded region. They concluded that lap joints between copper and aluminum is successful by friction stir welding. It was observed that near Al/Cu interface, an intermetallic compound of AlCu, Al_4Cu_9 and Al_2Cu was present and from there crack propagates during tensile testing.

An investigation was done on welding AISI 304 stainless steel and DHP copper by Zumelzu and Cabezas [48] in sea water environment. Welding process used were oxyacetylene and tungsten inert gas welding. Strain distribution and hardness strength were studied. Results obtained showed satisfactory weld between 304 stainless steel and DHP Copper. Sahin [49] investigated welding of steel bars with copper using friction stir welding. Sahin found out that growth of HAZ and

diffusion process is largely dependent on the temperature variation at the interface. Diffusion is greater when temperature is higher. He concluded that different metals can be joined using FSW. Mai and Spowage [2] investigated laser welding of Copper to Steel, Steel to Kovar and Copper to Aluminum using pulsed Nd:YAG laser. They concluded that in order to obtain a defect free joint, melting ratios of two metals should be controlled. As laser welding has higher power density, it allows a reduce interaction and control heat distribution which results in restricting brittle intermetallic phases.

A study on joining aluminum and steel was carried out by Mathieu [50] using laser beam welding. Steel and aluminum can't be joined using MIG or TIG due to the formation of brittle intermetallic compounds. Al 6016 and low carbon steel (zinc coated) were used with a filler wire of Zinc 85% and Aluminum 15%. Tensile tests showed satisfactory results. Fracture strength of the joints were evaluated and found to be 200 N/mm. In some conditions, rupture occurs in steels sheets and in the HAZ of aluminum. Liu [51] investigated laser welding of dissimilar materials between plates of alloy steel 42CrMo and Ni-based alloy K-418 using Continuous Nd:YAG laser. Microstructure was investigated using XRD, OM, SEM and EDS. Micro hardness and tensile testing was also done. Successful weld was obtained by adjusting flow rate of shielding gas, welding velocity and defocusing distance. Micro hardness showed to be lower than base metal. Strength of the joint was equal to base metal.

Chapter 3

Material and Experimental Work

2.5 Design of Experiment

Design of experiment is an orderly approach for investigation of a process or system. Planned changes are made in input parameters of system or process and series of assembled tests are designed. Results of these variations on pre-defined output are then evaluated. Design of experiments is important to maximize information obtained while minimizing aid required. Design of experiments are normally carried out in 4 phases. Planning, screening, optimization and verification.

3.1.1 Taguchi Design

Taguchi design provide an efficient and powerful method for designing commodity that operate optimally and consistently over a variety of conditions. Primary goal in taguchi design is to find factor settings that reduces response changes, while keeping the process on target. In this way of designing goal will produces consistent output.

Orthogonal arrays are utilized by taguchi design to study different number of variables and deducing less number of experiments. Examples of stand orthogonal arrays are

L-4, L-8, L-12, L-16, L-32 and L-64 all at 2 levels

L-9, L-18 and L-27 at 3 & 2 levels

L-16 and L-32 modified at 4 levels

L-25 at 5 levels

Standard notations for orthogonal arrays:

L-32 (2 4), 32 = Number of experiments

2 = Number of levels

4 = Number of factors

First, degree of freedom is to be known and then appropriate orthogonal array is to be fit. Laser parameters on which process depends were

- Laser Scan Speed
- Filler Materials

Speed variation was from 300 mm/min to 100 mm/min. Filler materials used were Nickel, Aluminium and Copper and without filler. Power is same in all cases that's why it will not be included in the changing parameter.

No of Parameters = 2, Number of States = 5

According to Taguchi's Method, L25 array will be used. Since there were only two parameters so we will take first two columns of L25. Total of 25 experiments were carried out to optimize the process parameter of laser welding of titanium Ti-6Al-4V and stainless steel 316L. Sample pattern and design of experiment is shown in Table 3.1 and Table 3.2.

Table 3.1 Sample Pattern

Experiment	**P1**	**P2**
1	1	1
2	1	2
3	1	3

4	1	4
5	1	5
6	2	1
7	2	2
8	2	3
9	2	4
10	2	5
11	3	1
12	3	2
13	3	3
14	3	4
15	3	5
16	4	1
17	4	2
18	4	3
19	4	4
20	4	5
21	5	1
22	5	2
23	5	3
24	5	4
25	5	5

Table 3.2 Design of Experiments

Experiment No	**Speed(mm/min)**	**Filler**
1	300	Nickel
2	300	Aluminum
3	300	Copper
4	300	No Filler
5	300	Nickel
6	250	Nickel
7	250	Aluminum
8	250	Copper
9	250	No Filler
10	250	Aluminum

11	200	Nickel
12	200	Aluminum
13	200	Copper
14	200	No Filler
15	200	Copper
16	150	Nickel
17	150	Aluminum
18	150	Copper
19	150	No Filler
20	150	No Filler
21	100	Nickel
22	100	Aluminum
23	100	Copper
24	100	No Filler
25	100	Aluminum

3.2 Materials

3.2.1 Materials Specifications

The materials selected for welding by CO_2 laser are as follows.

- **Stainless Steel 316L**

  Plate thickness of 1 mm are used. Width and length of plates are 40 x 55 mm.

- **Titanium 6Al4V**

  Plate thickness of 1mm are used. Width and length of plates are 40 x 55 mm.

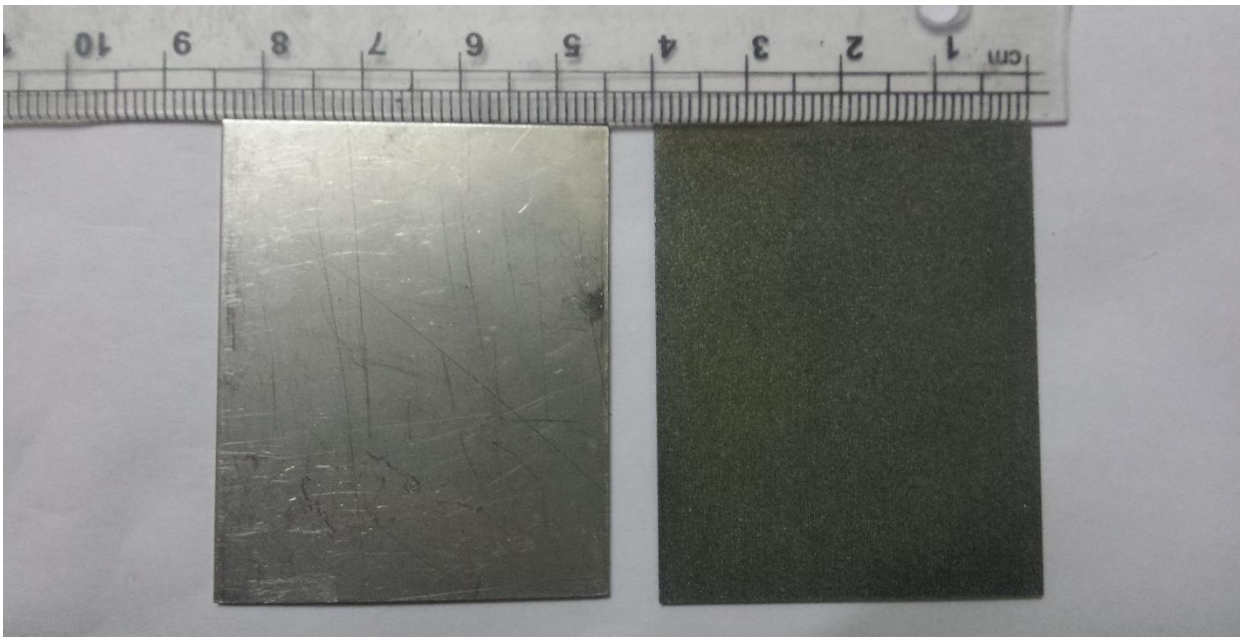

Figure 3.1: Samples Titanium Ti-6Al-4V (Left), Stainless Steel 316L (Right)

Chemical composition of materials were checked by X-ray fluorescence (XRF). The results obtained from XRF were comparable to the standard of their respective grades. Chemical compositions of titanium and stainless steel are presented in Table 3.3 and Table 3.4.

Table 3.3: Chemical composition of Titanium 6Al4V (wt %)

Material	Ti	V	Al	Cr	Cu	Fe	Mn
Titanium 6Al4V	89.4	4.30	6.15	.0027	.0045	.0510	.0055

Table 3.4: Chemical composition of Stainless Steel 316L (wt %)

Material	Fe	Cr	Mb	Mn	Co	Ni	Cu	C
Stainless Steel 316L	70.17	16.54	1.5	0.80	0.01	10.24	0.14	0.02

Standard mechanical and physical properties of Stainless Steel 316L and Titanium 6Al4V are presented in Table 3.5, 3.6, 3.7and 3.8 respectively.

Table 3.5: Mechanical properties of Stainless Steel 316L

Material	Tensile Strength (MPa) min	Yield Strength 0.2 % Proof (MPa) min	Elongation (% in 50 mm) min	Hardness Brinell (HB) max
Stainless Steel 316L	485	170	40	217

Table 3.6: Physical properties of Stainless Steel 316L

Material	Density (kg/m^3)	Elastic Modulus (GPa)	Mean Co-eff of Thermal Expansion 0-538°C (µm/m.°C)	Thermal Conductivity (W/m.K) At 500 °C	Specific Heat 0-100 °C (J/Kg.K)
Stainless Steel 316L	8000	193	17.5	21.5	500

Table 3.7: Mechanical properties of Titanium 6Al-4V

Material	Tensile Strength Mpa	Yield Strength (MPa)	Poisson's Ratio	Elastic Modulus GPa	Shear Modulus GPa	Hardness Brinell HB max
Titanium 6Al-4V	≥895	≥828	0.31	105-120	41-45	334

Table 3.8: Physical properties of Titanium 6Al-4V

Material	Density (g/cm^3)	Melting Point (°C)	Thermal Conductivity (W/m.K)	Specific Heat Capacity (J/g.°C)	Co-eff of Thermal Expansion 0-500°C (µm/m.°C)
Titanium 6Al-4V	4.43	1674	6.7	0.5263	9.7

3.3 Description and Use of the Studied Materials

Stainless steel grade 316 is molybdenum-bearing grade. As compared to 304, molybdenum provides 316 excellent corrosion resistant, minimum corrosion in chloride environment and inflated resistance to pitting. Grade 316L is extra low version of 316 and provide immunity to carbide precipitation during welding and is highly suitable for welding. This grade has excellent toughness, even near to cryogenic temperatures due to austenitic structures. Stainless steel 316 has wide applications including furnace parts, pharmaceutical equipment, chemical equipment, valve and pump trim, digesters, textile processing equipment, jet engine parts, exhaust manifolds, photographic equipment, and evaporators.

Titanium Grade 5 Ti-6Al-4V is alpha beta alloy of titanium and is the most commonly used alloy of titanium. Heat treating can be used to increase its strength. Ti 6Al-4V offers light weight, high strength to weight ratio, formability and excellent corrosion resistance. The service temperature of this grade is 350°C. This grade has wide applications and used in gas turbine engine components, military airframe parts, nuclear power plants, heat exchangers of oil refinery, medical prostheses and marine components.

3.4 Joint Design and Preparation

The samples were welded using butt joint configuration in which samples are placed parallel to each other. In fusion welded joints, butt joints are used preferably. Sample preparation started with cleaning of sheets using emery paper (grade 240). Edges were preferably cleaned where the two samples assembled. Edges of the plates were well prepared in order to ensure complete contact between the plates. As in order to achieve successful welding in butt joint configuration, complete contact between the plates is necessary otherwise laser will pass through any gap left between the samples and proper welding won't be achievable. To ensure complete contact, surface grinder was used. All samples were grinded first to ensure complete contact.

Figure 3.2: Surface Grinder

Ethanol C_2H_5OH which is volatile, colorless and flammable liquid was used to clean the samples prior to welding. All samples were carefully cleaned in order to avoid any contamination that may

result in failure of weld. Titanium is extremely sensitive to contamination. During welding of titanium oxygen, nitrogen, carbon and hydrogen get absorb in it and embrittle it. Proper care was employed to ensure that it don't get contaminated. Hydrogen and carbon was eliminated by cleaning it with ethanol. Gloves were used to hold the titanium as even bare hands have oil that can contaminate it. Oil was removed from the samples by first washing it with soap and then using ethanol to completely clean it. Nitrogen and oxygen was eliminated using proper gas shielding.

Different filler materials were used in the study. Aluminium, copper and nickel were used as filler materials. Thickness of 0.2mm was used. Pictures of filler materials are shown below.

Figure 3.3: Filler Materials Aluminum (Left), Copper (Right)

A fixture was used to hold the plates together during laser welding. Fixture was employed in order to hold the samples tightly in their respective positions and also to elude any thermal deformation due to heat input.

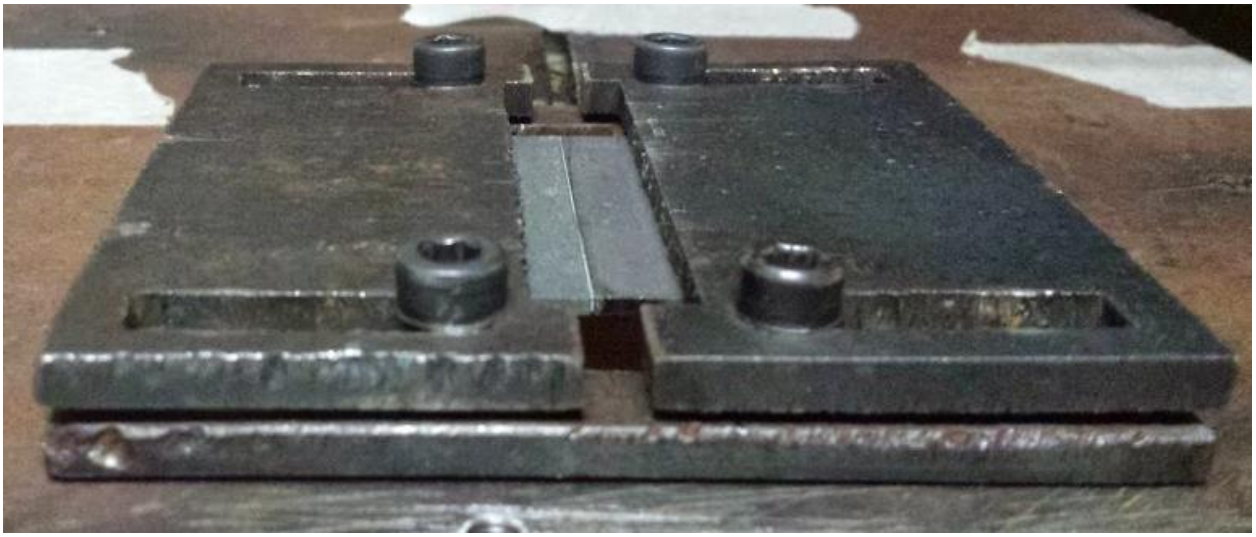

Figure 3.4: Fixture used for clamping samples during laser welding

3.5 Preheating of samples

All the samples were preheated immediately before welding in order to raise the temperature of the samples. Preheating is done in order to slow down the cooling rate of the weld. This protects the materials from any adverse effects including cracking due to thermal stresses and in heat affected zone. Another important reason for preheating was welding titanium requires moisture to be omitted completely as titanium is very reactive at high temperature so preheating is done to remove moisture. There are number of ways through which preheating can be applied. Applying preheating depends on sample thickness, heating equipment available and weldment size. It is necessary to apply preheat correctly and to ensure temperature doesn't fall below the preheat temperature. Samples were preheated to 200°C using hot air blower after clamping the samples

in the fixture. Proper care was carried out to ensure the temperature of the samples don't fall below the preheat temperature.

Figure 3.5: Hot Air Blower

A digital thermometer was used to check heated samples after preheating to ensure that required preheated temperature is achieved. Temperature range of thermometer was -200℃ to 1200℃.

Figure 3.6: Digital Thermometer

3.6 Shrouding System Design

Proper shrouding system was made to cover the melt and to eliminate the air from the weld zone in order to avoid brittle intermetallic as titanium is very reactive to oxygen and nitrogen. Argon gas was used for shielding purpose. Shrouding system was designed to secure the samples without affecting flow rates. In order to avoid brittle intermetallic in titanium, gas shielding should be provided from the bottom as well. So for this purpose, gas shielding was provided from the top and the bottom side. Movable shading gas was fluttered from the laser head and it moves along the laser head during the welding. Second shielding gas was provided at the bottom. A tube was extended from the main supply of shielding gas and a nozzle of 2mm diameter was attached. The nozzle was attached below the sample fixture at an angle of 45^{o}.

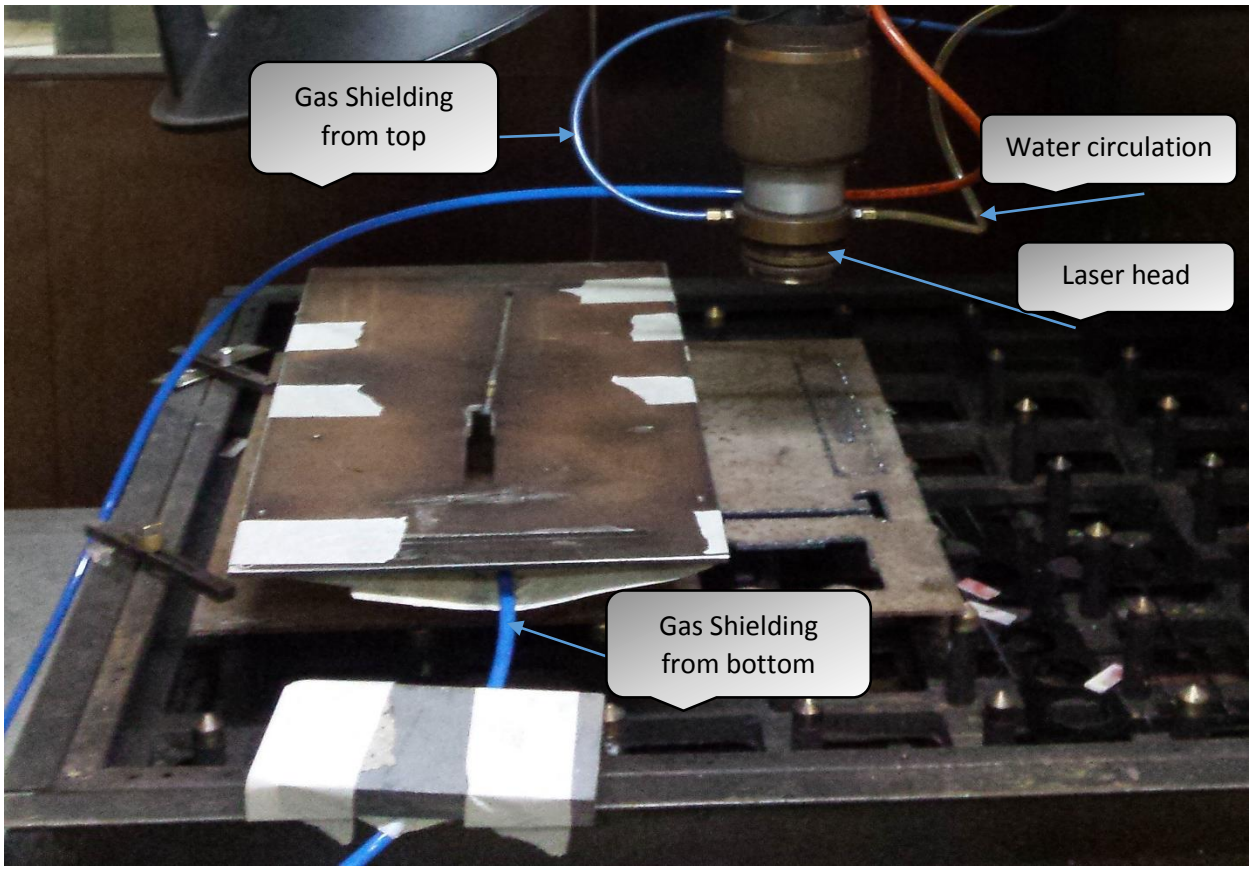

Figure 3.7: Shrouding system

Basic purpose of the shielding was to protect the welding area from water vapors and oxygen. Improper selection of welding gas can lead to failure or weak weld. In laser welding, shielding has one additional role as well. It prevent the development of plasma cloud just right above the weld. Inert gases are used for shielding purpose. Helium is lighter than air so higher flow rate are required to completely shield the sample. It is expensive as well. Argon is cheaper and denser than helium so argon gas was selected as shieling gas. The pressure of argon gas was maintained at 3 bar.

Figure 3.8: Argon Gas cylinder

3.7 Laser Welding

After preparing samples and setting shrouding system, CO_2 laser was used for welding of samples.

3.7.1 Laser Welding Machine

CO_2 laser (HJ-2500) with a maximum power of 2.5KW and 10.6µm was used as shown in Figure 3.9. The technical specifications are mentioned in Table 3.7. The laser system (Two dimension moving table, laser cooling system, air compressor, chillers, and control software) was provided by Pakistan Institute of Laser Optics (PILO). Schematic diagram of laser machine is shown in Figure 3.10. Speed range of system varies from 10mm/min to 2000mm/min. Spot size of laser beam is 0.3mm. For welding, lens of focal length 80mm was used. Gas pressure is maintained at 85Torr. A mixture of laser gas is used for operating the CO_2 laser machine. The gas mixture ratio is CO_2: N_2: He = 1: 8: 1. Self-Contained Air Cooled Chiller is used for cooling. Technical specifications are mentioned in Table 3.8.

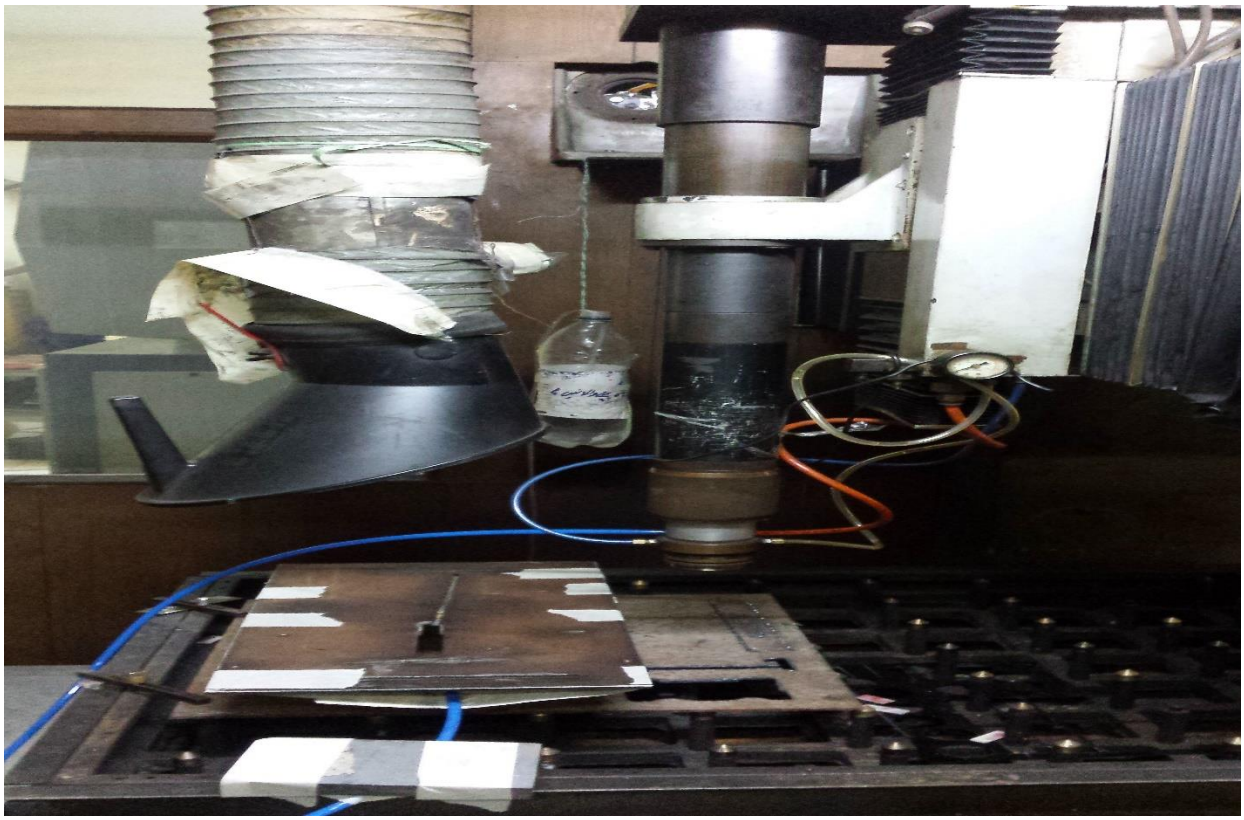

Figure 3.9: HJ-2500 CO_2 Laser Machine

Table 3.7: Specifications of HJ-2500 CO_2 Laser

Technical Data	HJ-2500
Output Power	2500W
Power Range	50-2500W
Beam quality factor	K>0,9
Gas Pressure	11.33KPa
Gas Mixture	CO_2: N_2: He
Temperature of Cooling Water	20°C
Pressure of Cooling Water	0.1-0.2MPa

Table 3.8: Specifications of Air Cooled Chiller

Technical Data	Air Cooled Chiller
Nominal Cooling Capacity	98000 Btu/Hr
Chiller Water Flow Rate	19.4 US Gpm
Power Supply	380/415-3-50Hz
Refrigerant	R-22
Compressor Current	0.9 RLA

Experimental setup of the CO_2 laser is shown below.

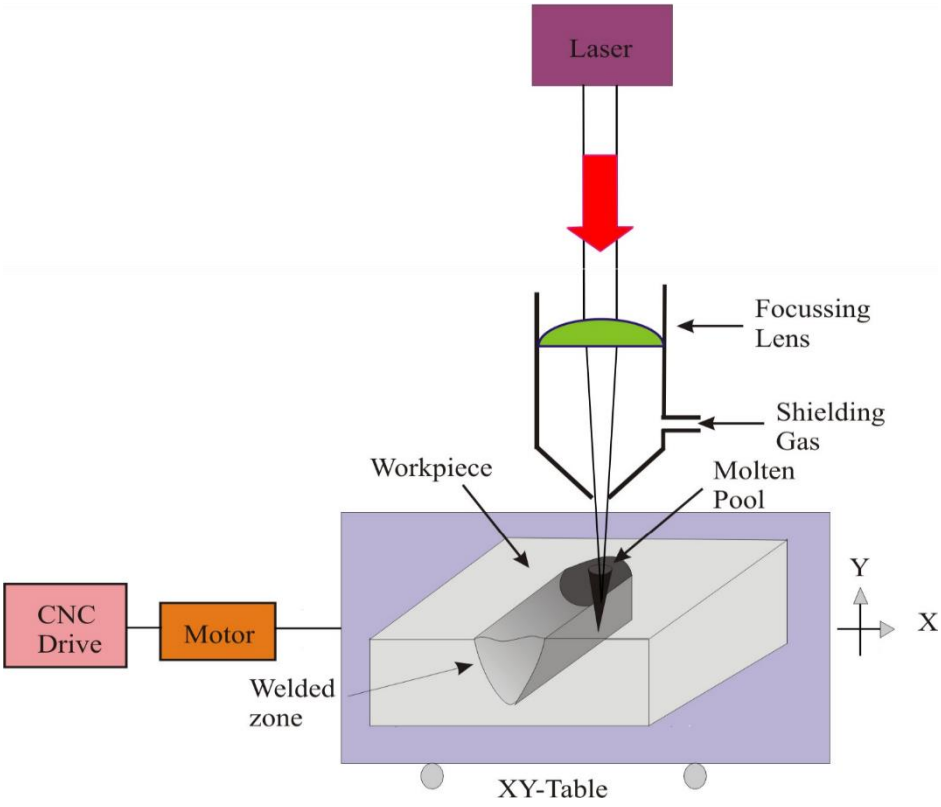

Figure 3.10: Experimental set up for laser welding process.

3.8 Laser Welding Operations

Initial experiments were carried out in Pakistan Institute of Laser Optics (PILO) to determine operating range of welding parameters in order to make admissible quality welding of dissimilar metals. First, bead on plate on titanium and stainless steel samples were carried out. After that, dissimilar metal welding was carried out between stainless steel and titanium using copper, aluminum and nickel as filler materials. Autogenous welding was also performed. Visual inspections were made to decide the operating range. Visual inspections include cracks, misalignments, full penetration and poorly formed beads. Once the parameters got set,

experiments were design using taguchi method. After that, experiments were carried out with and without use of filler materials. Samples were fixed in the fixture to avoid any thermal deformation due to heat input. Preheating was done with the help of blower.

3.9 Initial Experimentation

First of all, bead on plate was carried out on SS-316L and Ti-6Al-4V to get the required suitable welding parameters. Laser power of 650W and scan speed ranging from 300 mm/min to 100 mm/min was used. Thermal diffusivity of Ti is 6.9e-6 m2/s and for SS is 4.08e-6 m2/s i.e. almost twice than SS. Also Ti has higher melting temperature of 1665 ^{o}C and SS has 1375 ^{o}C. So in order to properly melt the samples, laser beam was offset 0.2mm on titanium side. Effect of scan speed on microstructure was investigated as well. Penetration of weld using different scan speed was also studied. After that, butt joint configuration was used to weld the samples and three types of filler materials were used. Aluminum, Copper and Nickel were used as filler materials. Thickness of all filler materials were 0.2 mm. First, autogenous welding was done and then with the above mentioned fillers.

3.9.1 Laser welding without any filler

Autogenous welding of stainless steel 316L and Titanium Ti-6Al-4V was performed. Laser power of 650W and scan speed of 300 mm/min was used. 6 samples were welded using these parameters. Pictures of the samples are shown in figure 3.11.

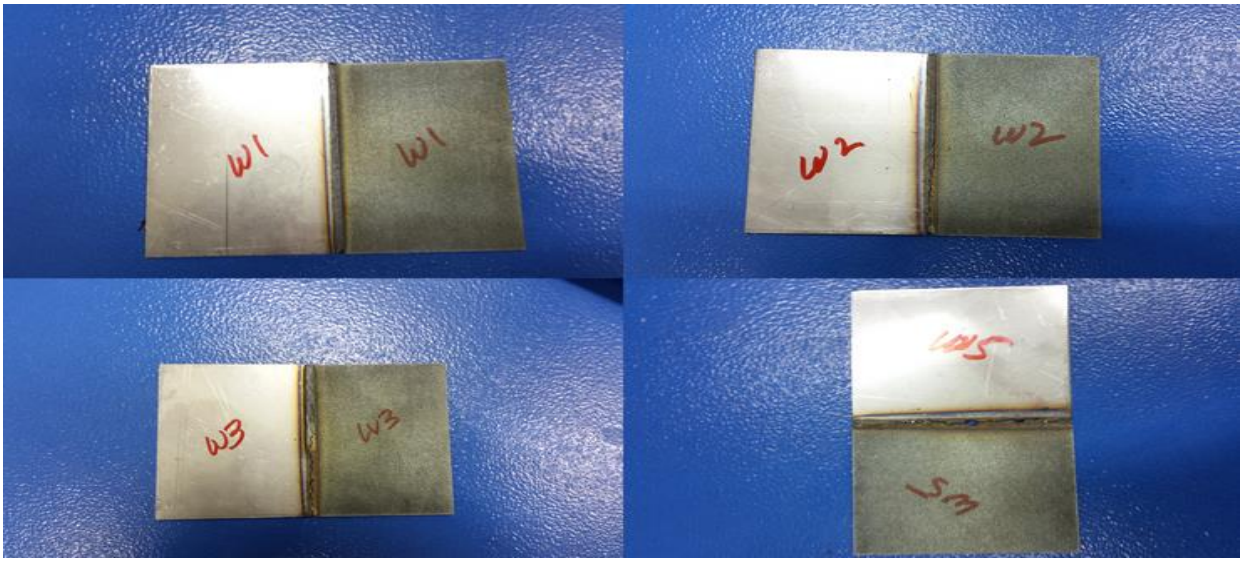

Figure 3.11: Laser welding of SS-Ti without filler

3.9.2 Laser welding using Copper as filler

Laser welding of stainless steel 316L and Titanium Ti-6Al-4V was performed using copper as a filler material. Thickness of filler was 0.2mm. Laser power of 650W and scan speed of 300 mm/min was used. 6 samples were welded using these parameters. Pictures of the samples are shown in figure 3.12.

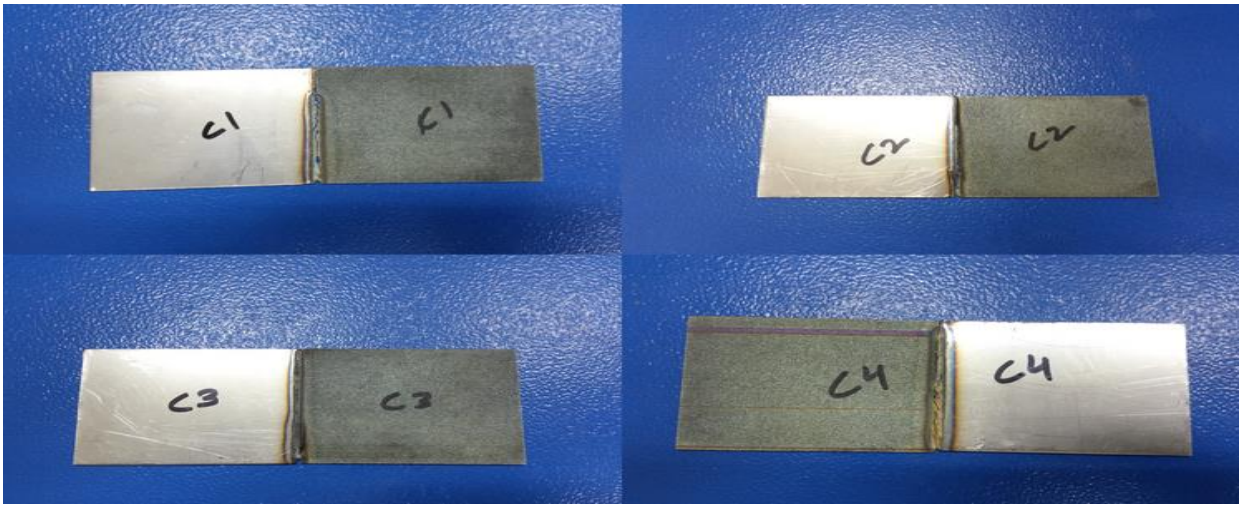

Figure 3.12: Laser welding of SS-Ti with Copper as filler

3.9.3 Laser welding using Aluminium as filler

Laser welding of stainless steel 316L and Titanium Ti-6Al-4V was performed using aluminium as a filler material. Thickness of filler was 0.2mm. Laser power of 650W and scan speed of 300 mm/min was used. 6 samples were welded using these parameters. Pictures of the samples are shown in figure 3.13

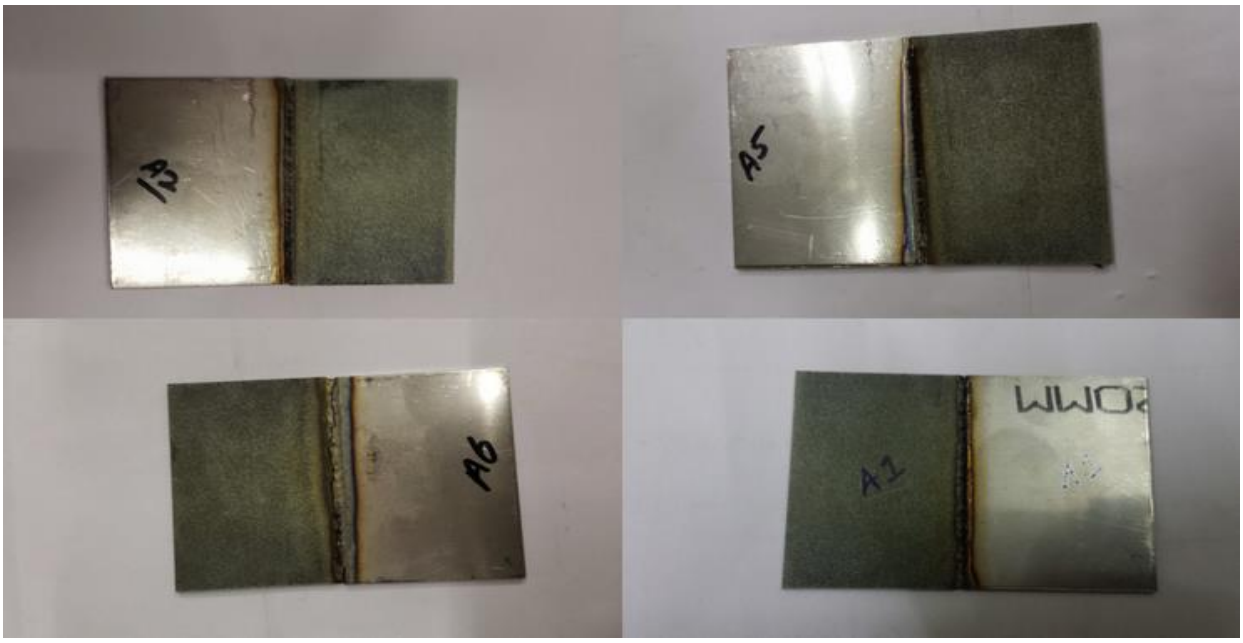

Figure 3.13: Laser welding of SS-Ti with Aluminium as filler

3.9.4 Laser welding using Nickel as filler

Laser welding of stainless steel 316L and Titanium Ti-6Al-4V was performed using nickel as a filler material. Thickness of filler was 0.2mm. Laser power of 650W and scan speed of 300 mm/min was used. 6 samples were welded using these parameters. Pictures of the samples are shown in figure 3.15.

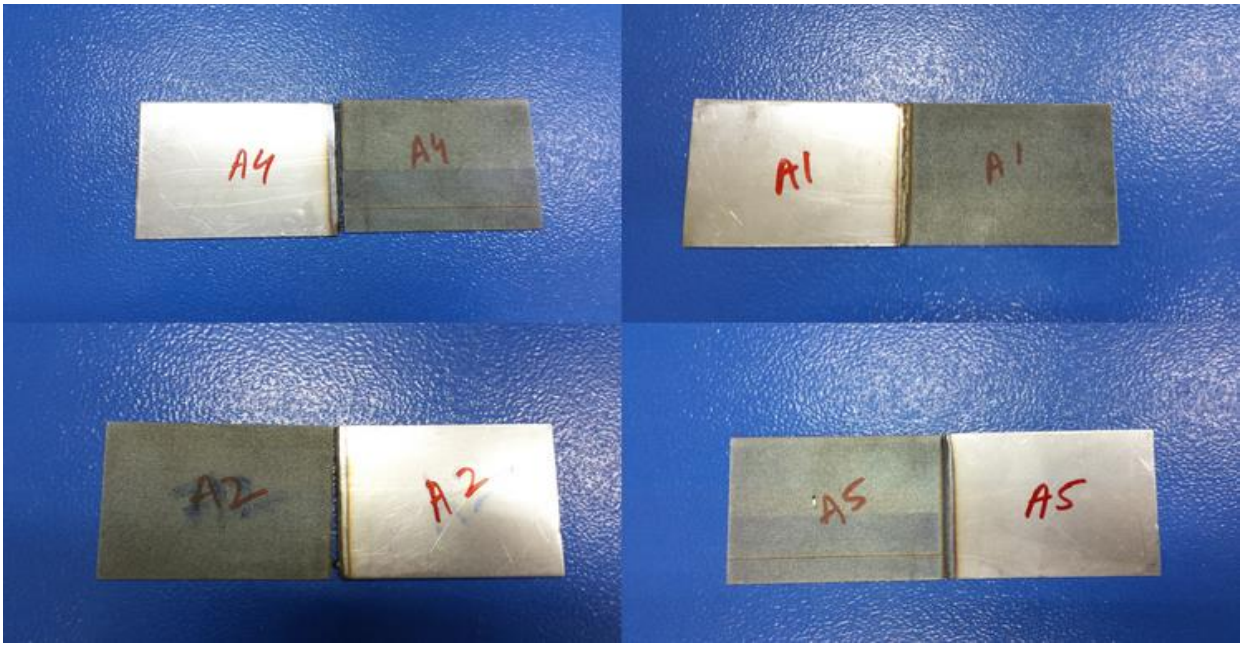

Figure 3.15: Laser welding of SS-Ti with Nickel as filler

3.10 Micro-Study and Weld Pool Geometry Determination

3.10.1 Sample Preparation

A small sample was obtained from every welded sample cut perpendicular to the direction of weld using Electric Discharge Machining including with and without filler welded samples to study the geometry and shape of weld pool. Mounting press (Mekton) was used to mount the welded samples for grinding and polishing. Grinding was done on grinding machine with silicon carbide paper of range (120, 240, 400, 800 and 1200) grains/cm^2. Samples were grinded for five minutes for each grade, at speed of 350 rpm. Water was used for cooling. Polishing was done using diamond paste of varying grain size. First grain size of 6µm, then 3 µm and 1 µm was used. Samples were polished for five minutes for each grade. Samples were cleaned using acetone and then dried using hot air blower. For etching Titanium Ti-6Al-4V, Kroll's reagent (distilled water 92ml, HNO_3 6ml, HF 2ml) was used. Stainless Steel 316L was etched with Glyceregia (Glycerin

30ml, HCl 20ml, CH_3OOH 10ml, HNO_3). Titanium samples were immersed in solution for 1-3 seconds. Stainless steel samples were swabbed for 2-3 minutes to show properly the grain boundaries.

3.10.2 Microstructure

Optical microscope (Olympus PMG 3) with video camera was used to inspect the microstructure of dissimilar welded joints shown in Figure 3.16.

Figure 3.16: Metallurgical Optical Microscope

3.11 Weld Pool Geometry

Optical microscope was used to measure the area of welding zone .Welding pool width and depth was measured. Average of four or more results of weld geometry were measured and ordered for further analysis.

3.12 Hardness

Hardness of bead on plate weld and dissimilar material weld were calculated using Vicker Micro Hardness Testing Machine DIN 51033 as shown in Figure 3.17. Load of 6Kg was put on for 30 seconds and then indentations were calculated. The distance between the measuring points were 100mm. Indentations were calculated across bead on plate weld and welded samples of stainless steel 316L and titanium Ti-6Al-4V. An average of three reading were taken for each location of weld sample and put in table for further studies. Formula used for calculating vicker hardness number is as follows.

HV = $1.8544 \times p/d2$ Where p = load in Kgf, d = indentation in mm

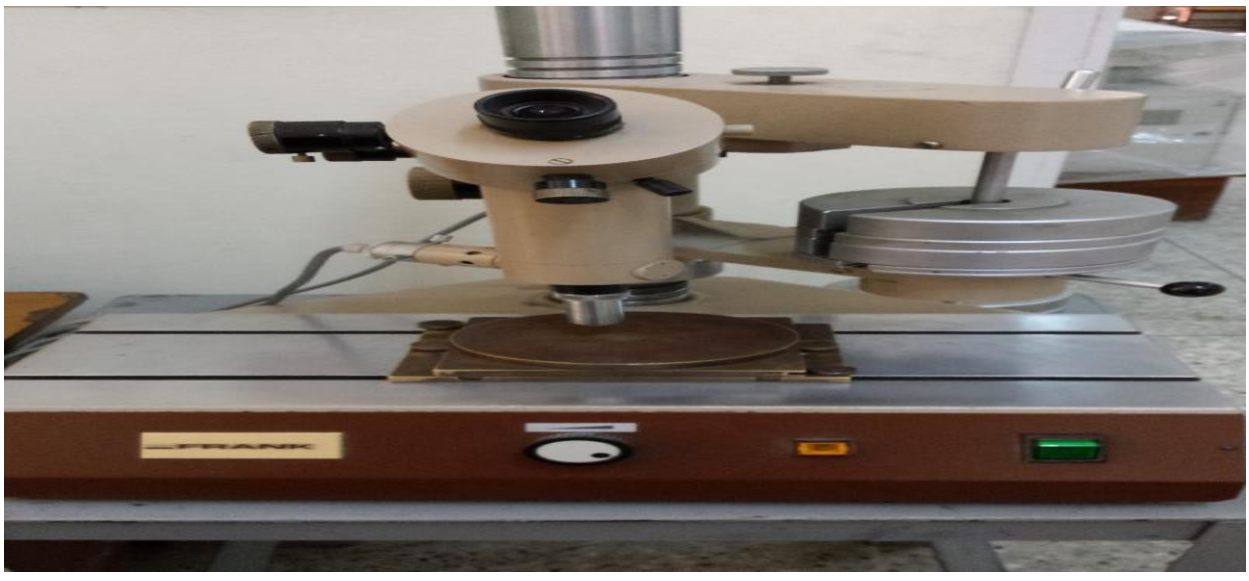

Figure 3.17: Vicker Micro Hardness Testing Machine

Chapter 4

Result and Discussions

This chapter will give the results and discussion of dissimilar laser butt welding of Stainless steel 316L and Titanium Ti-6Al-4V.

4.1 Effect of transverse speed on weld depth and width

Bead on plate weld were performed on stainless steel 316L and titanium Ti-6Al-4V samples at 650W and varying scan speed ranging from 300 mm/min to 100 mm/min. Focused laser beam of 0.3mm spot size was used that produces continuous blue flash. Figure 4.1 and Figure 4.2 shows graph for width and depth of laser treated zone and scan speed for bead on plate weld for Ti and SS. It was observed that weld depth and width was increased by decreasing the scan speed. As we increased the scan speed, the interaction time of laser beam with the material reduces which decrease the heat input in the sample.

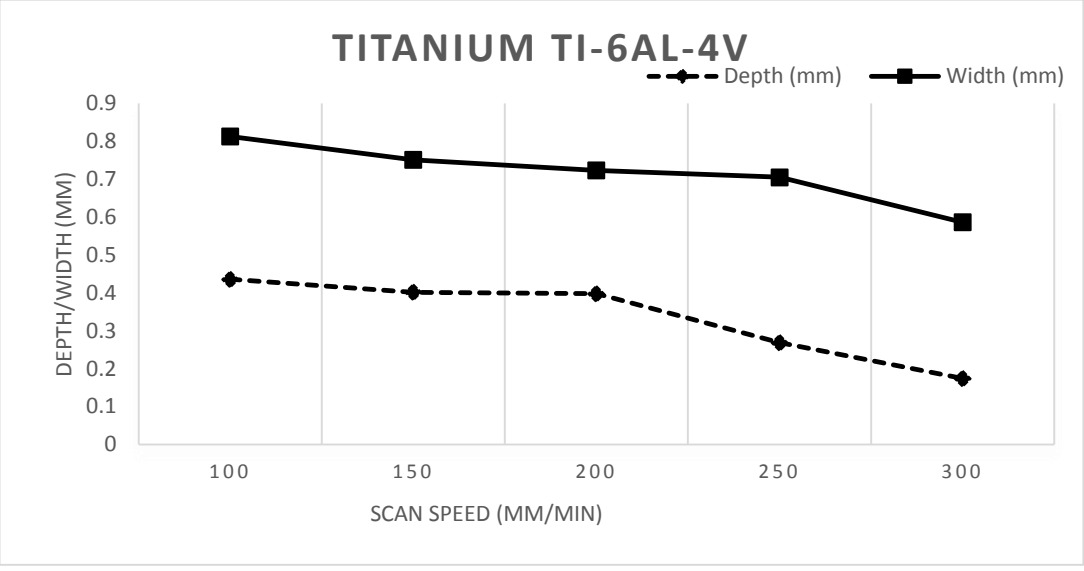

Figure 4.1: Variation of weld width/depth at different scan speeds at laser power of 650W.

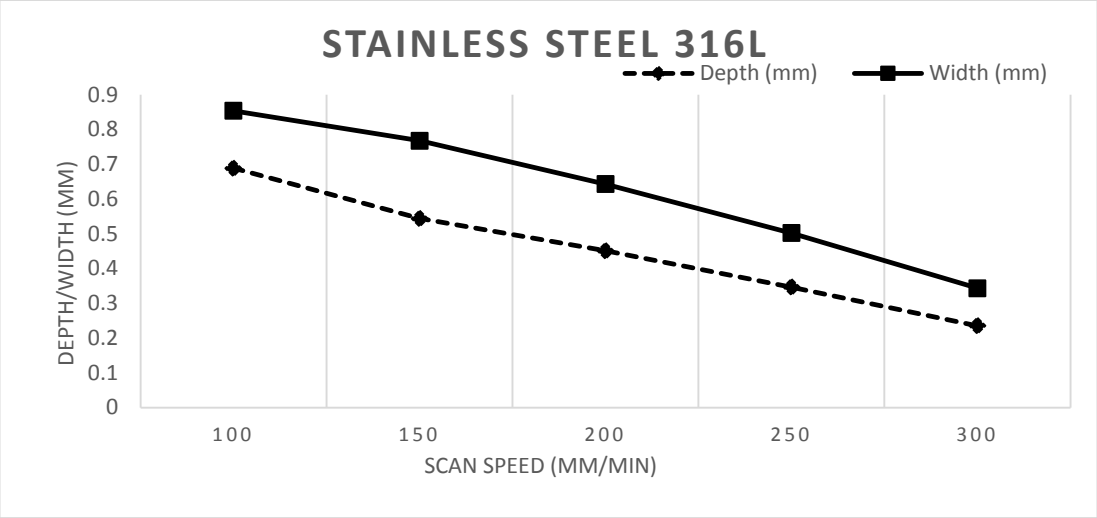

Figure 4.2: Variation of weld width/depth at different scan speeds at laser power of 650W.

4.2 Hardness variation across the Beads on Plate Weld Samples

Hardness test of stainless steel and titanium using Vicker Hardness Testing Machine showed variation of hardness across the beads made by varying scan speed. Hardness profiles were documented to check the effect of welding process on structure of metal because variation of microstructure are known to result in changing hardness of the metal.

4.2.1 Titanium Ti-6Al-4V

Table 4.1 shows variation of hardness across the weld zone of Titanium Ti-6Al-4V and graph was plotted between Scan Speed and Micro Hardness value (DPH) for titanium Ti-6Al-4V as shown in Figure 4.3.

Table 4.1 Hardness values for Titanium Ti-6Al-4V

Sample Ti-6Al-4V	Scan Speed (mm/min)	P (kg)	L (mm)	L^2 (mm^2)	DPH (kgf/mm^2)
Base Plate	300	6	0.196	0.038416	289.5668471
HAZ	300	6	0.187	0.034969	318.1103263

Weld Zone	300	6	0.137	0.018769	592.6794182
Base Plate	250	6	0.196	0.038416	289.5668471
HAZ	250	6	0.1725	0.029756	373.8374291
Weld Zone	250	6	0.139	0.019321	575.746597
Base Plate	200	6	0.195	0.038025	292.5443787
HAZ	200	6	0.17	0.0289	384.9134948
Weld Zone	200	6	0.14	0.0196	567.5510204
Base Plate	150	6	0.195	0.038025	292.5443787
HAZ	150	6	0.179	0.032041	347.1801754
Weld Zone	150	6	0.14	0.0196	567.5510204
Base Plate	100	6	0.195	0.038025	292.5443787
HAZ	100	6	0.179	0.032041	347.1801754
Weld Zone	100	6	0.142	0.020164	551.6762547

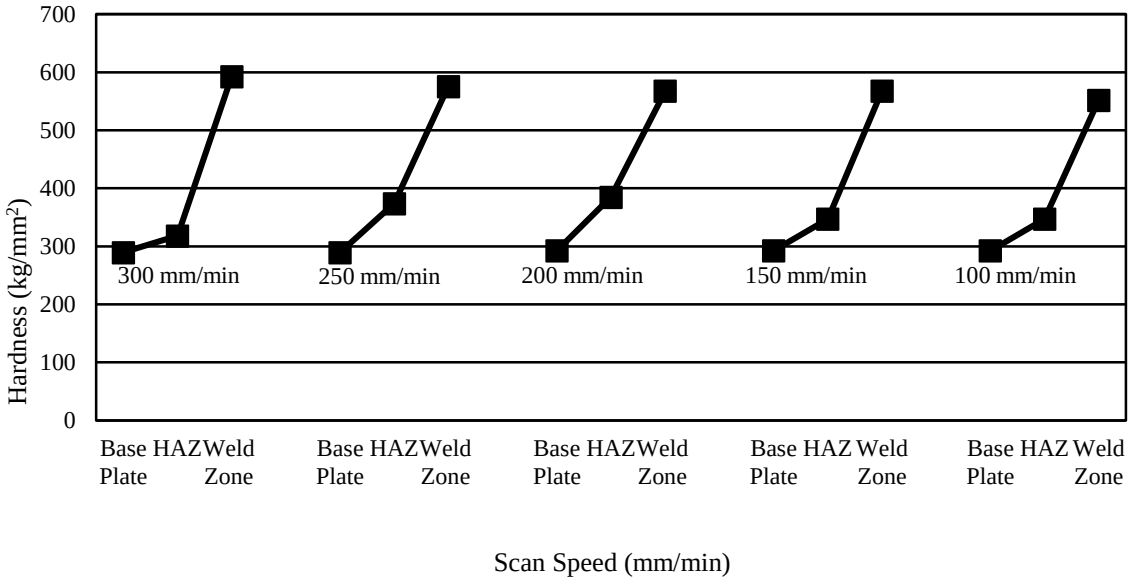

Figure 4.3: Hardness values for Titanium Ti-6Al-4V. Each data point represents mean value of three data point measurements.

Graph illustrates that hardness of titanium increases in heat affected zone and considerably higher in welded zone while in the base plate it didn't vary. Higher value of hardness is due to impurities like oxygen, hydrogen, carbon and nitrogen induced and due to rapid cooling. Another factor that is to be considered is, by decreasing the scan speed, there is no major variation in the hardness value. It is nearly equal to when bead on plate weld (Ti-6Al-4V) was performed with scan speed of 300 mm/min i.e. 592 DPH and when performed with scan speed of 100 mm/min i.e. 551 DPH. High significant differences were noted when comparing base metal with the weld zone.

4.2.2 Stainless Steel 316L

Table 4.2 shows variation of hardness across the weld zone of Stainless Steel 316L and graph was plotted between Scan Speed and Micro Hardness value (DPH) for Stainless Steel 316L as shown in Figure 4.4.

Table 4.2 Hardness values for Stainless Steel 316L

Sample SS-316L	Scan Speed (mm/min)	P (kg)	L (mm)	L^2 (mm^2)	DPH (kgf/mm^2)
Base Plate	300	6	0.266	0.070756	157.2163491
HAZ	300	6	0.246	0.060516	183.8191553
Weld Zone	300	6	0.258	0.066564	167.1173607
Base Plate	250	6	0.265	0.070225	158.4051264
HAZ	250	6	0.249	0.062001	179.416461
Weld Zone	250	6	0.269	0.072361	153.7292188
Base Plate	200	6	0.266	0.070756	157.2163491
HAZ	200	6	0.252	0.063504	175.170068
Weld Zone	200	6	0.26	0.0676	164.556213
Base Plate	150	6	0.264	0.069696	159.607438
HAZ	150	6	0.235	0.055225	201.4305115

Weld Zone	150	6	0.25	0.0625	177.984
Base Plate	100	6	0.264	0.069696	159.607438
HAZ	100	6	0.236	0.055696	199.7270899
Weld Zone	100	6	0.249	0.062001	179.416461

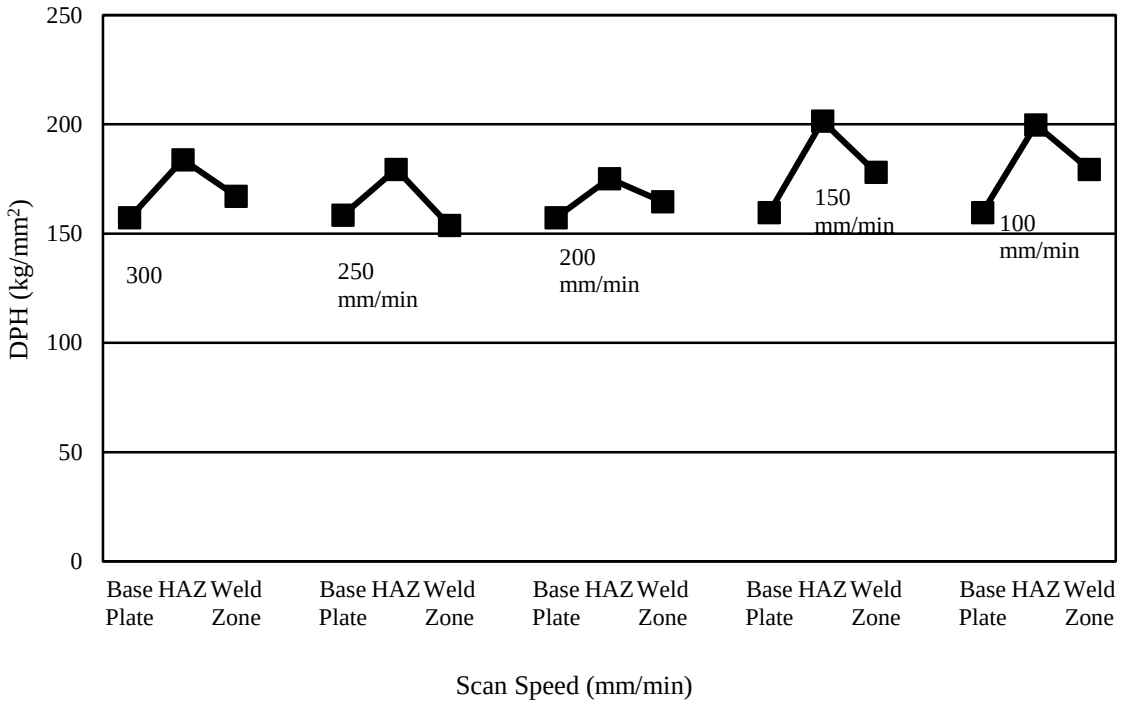

Figure 4.4: Hardness values for Stainless Steel 316L. Each data point represents mean value of three data point measurements.

Hardness profile of weld zone, HAZ and base plate of stainless steel 316L as function of scan speed is shown in Figure 4.4. No major difference between hardness of weld zone and heat affected zone was observed. By varying scan speed, no major difference in hardness values were obtained. At 200 mm/min, hardness of weld zone was 164 DPH while at 300 mm/min, hardness

of weld zone was 167 DPH. Hardness of HAZ is higher than base plate and weld zone. This is because of finer grains in HAZ due to rapid cooling as compared to base metal and welding zone. Similar results were reported previously [52, 53].

4.3 Equilibrium Phases of Fe-Ti Dissimilar Material Pair

The Ti-SS pair is not widely used in welding due to existence of numerous brittle intermetallics with in Iron-Titanium phase diagram. Stainless steel which is mainly composed of Cr, Fe and Ni will make many of these phases when fuse with titanium as study in Iron-Titanium material pair and that will have effect on ductility and mechanical strength. Expected two main components in Titanium-Stainless Steel material weld pair are shown in binary phase diagram [54] in Figure 4.5.

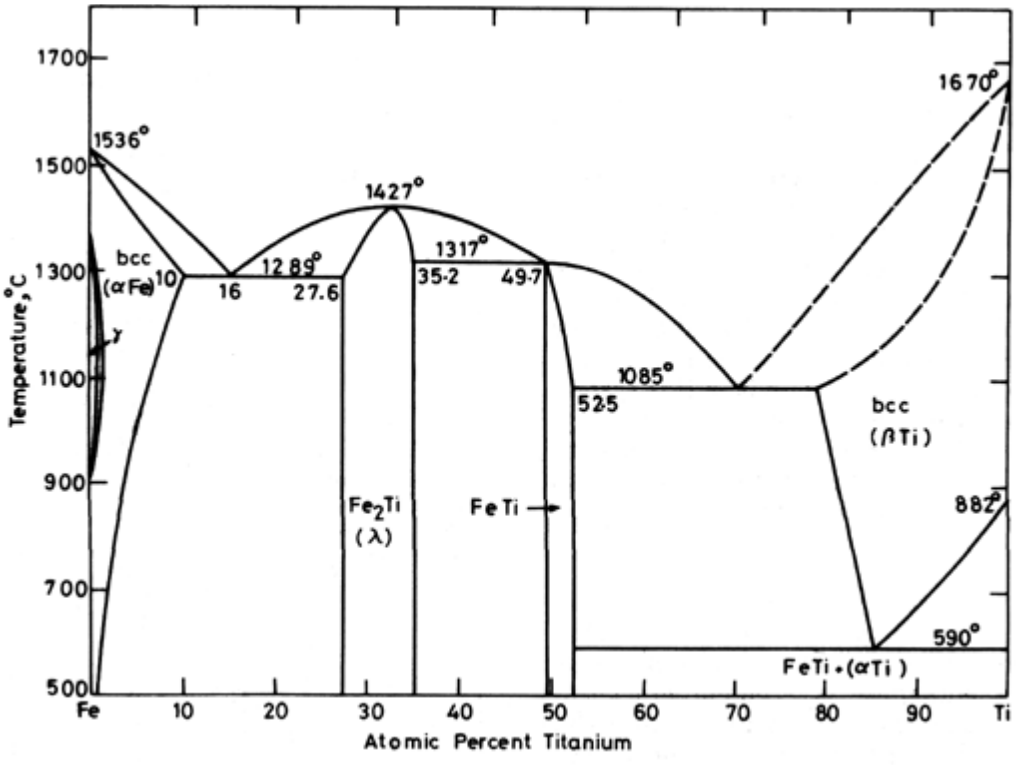

Figure 4.5: Iron-Titanium phase diagram giving at least two intermetallic phases in stainless steel-titanium pair.

There are two phases namely $NiTi_2$ and $TiCr_2$ are omitted in binary phase diagram which will form in small amounts in Ti-SS mixture. In binary phase diagram of Ti-SS, following phases are formed in order of decreasing iron content i.e. α-Fe, λ, FeTi, β-Ti and α-Ti. $TiFe_2$ represent λ that has C14 hexagonal Laves intermetallic structure. The λ-Lave phase homogeneity range is in between 72.4 and 64.8 at% Fe and has closed packed structure. β-Ti will transform into TiFe and α-Ti through eutectoid reaction and has base centered cube structure. α-Fe has base centered cube structure while FeTi has the same structure i.e. BCC. On the titanium rich side, TiFe and β-Ti are formed through the eutectic reaction upon cooling. A lamellar structure is obtained at equilibrium with alternating layers of TiFe and β-Ti. These layers are in the forms of plates have specific crystal orientation that's objective is to reduce the excess energy present between the two phases [13]. Directionality is noted at higher cooling rate as in laser welding that result in plates aligned in direction of heat flow. During solidification of eutectic composition, first solid solution of β-Ti will form and then FeTi intermetallic phase will form. Dendrites are in the form of TiFe and β-Ti will be in the form of matrix. The dendrites will preferably formed in the direction of heat flow [55]. The interfaces between matrix β-Ti and dendrites TiFe make the crack propagation to be captured. Secondly, the anisotropy introduced by the formation of orientated dendrites will affect the mechanical properties and it will show greater strength along the direction of growth of dendrite and reduce strength in transverse direction [56]. According to binary phase diagram, α-Ti will form below 595ºC. β phase can also be stabilized by alloying. There are number of elements that are β-stabilizers e.g. Ta, Fe, W, V, Mo and Cr. On the other hand, O and Al are α-stabilizers and their presence increase the α/β transus. So compositional change can stabilize β-phase. The solubility of iron in β-Ti is increased as well at high and rapid cooling rates [57]. These factors shows that single phase β-Ti (Fe) can be formed outside homogeneity range.

4.4 Weld geometry and microstructure

4.4.1 Laser welding of SS 316L and Ti-6Al-4V (Without filler)

The weld between SS 316L and Ti-6Al-4V shows the cross section of cracked welded sample processed at power of 650W. Proper penetration is achieved. Variation in the interface between SS and Ti was observed due to differences in material properties. The length of the HAZ at the Ti side is less (almost half) than on the SS side as shown in the Figure 4.6.

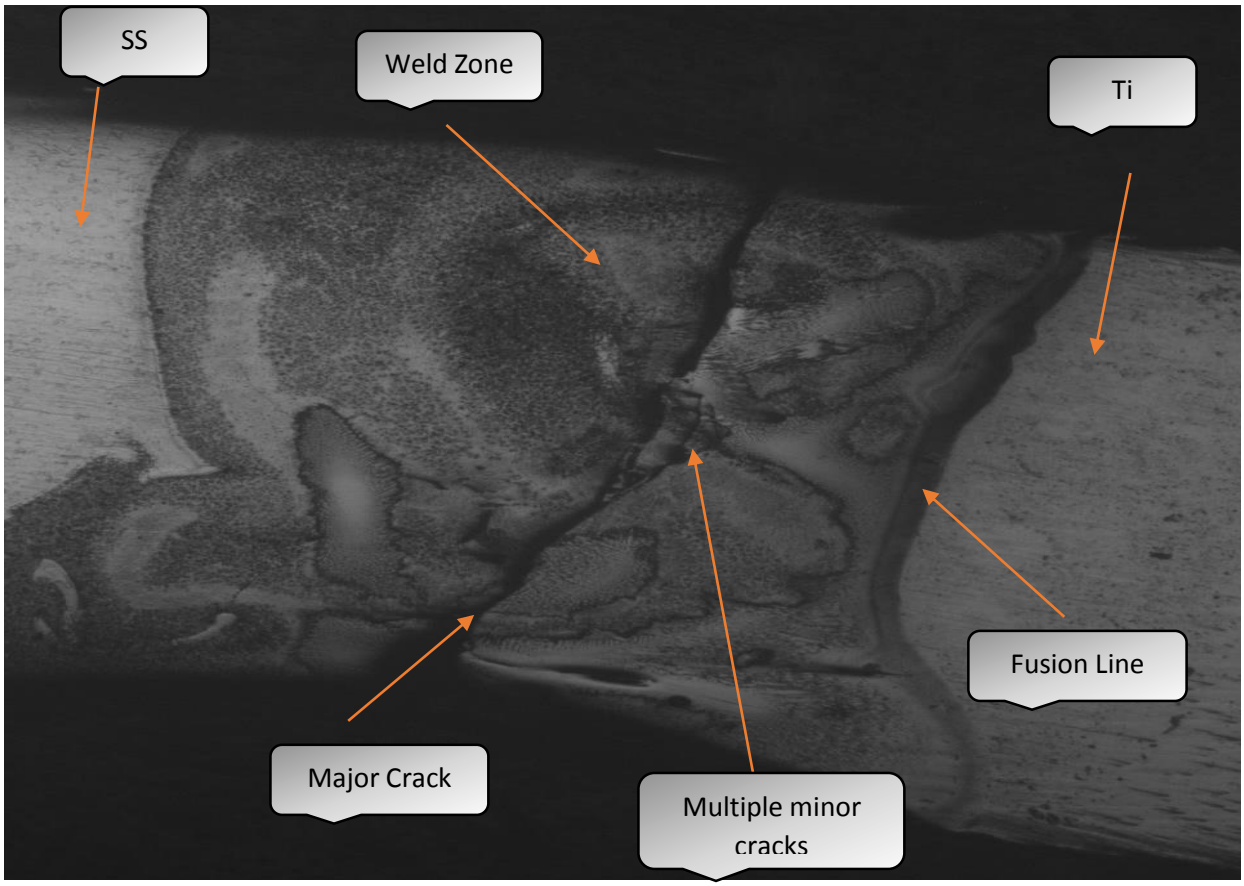

Figure 4.6: Weld cross-section (Without Filler). Note asymmetry of weld pool and presence of various microstructures in weld pool. Laser Power: 650W, Scan Speed: 300 mm/min.

Figure 4.7 (a), (b) and (c) shows optical micrographs of the parent stainless steel, titanium and fusion zone respectively.

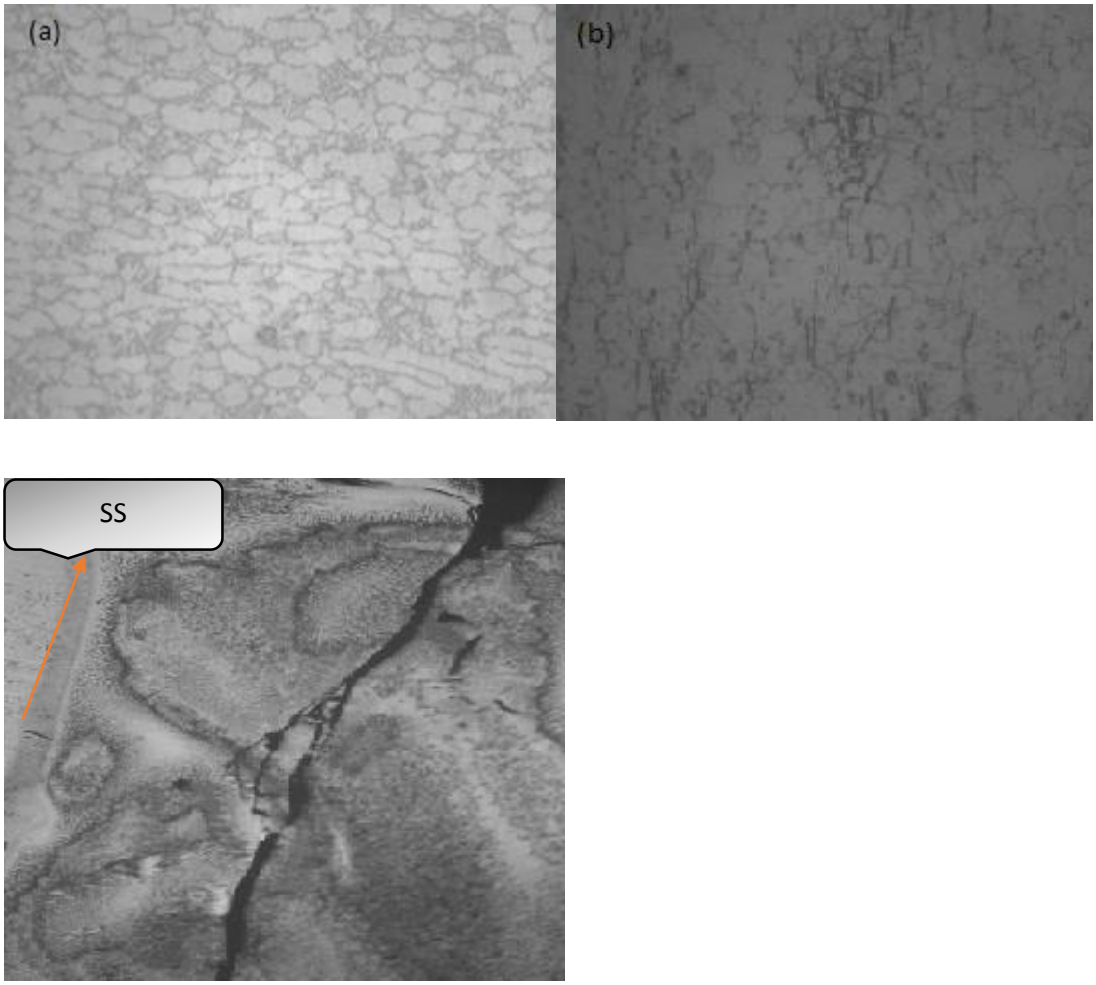

Figure 4.7: (a) Parent Ti metal (b) Parent SS metal (c) HAZ and fusion zone

During the freezing of molten metal, a tree like crystal structure is formed. These dendrites formed during cooling of molten metal has large effect on the properties of material. These dendrites are formed at the interface during the growth of solid in the weld pool. The interface of solid-liquid is determined by thermal and constitutional parameters. Depending on such conditions, the interface growth can made by cellular, planar or dendritic growth [58]. Dendrites are observed clearly in higher magnification optical micrograph at SS Side as shown in figure 4.8.

The solidification control the shape and size of grains, the distribution of porosity and inclusion and segregation [59]. Directional solidification is observed from the interface to the weld zone due to orientated dendrites existed normal to solid-liquid interface. From the figure 4.8, it was observed that diffuse and broad zone is produced as the reason for such behavior is that the interface is not sharp at the SS side.

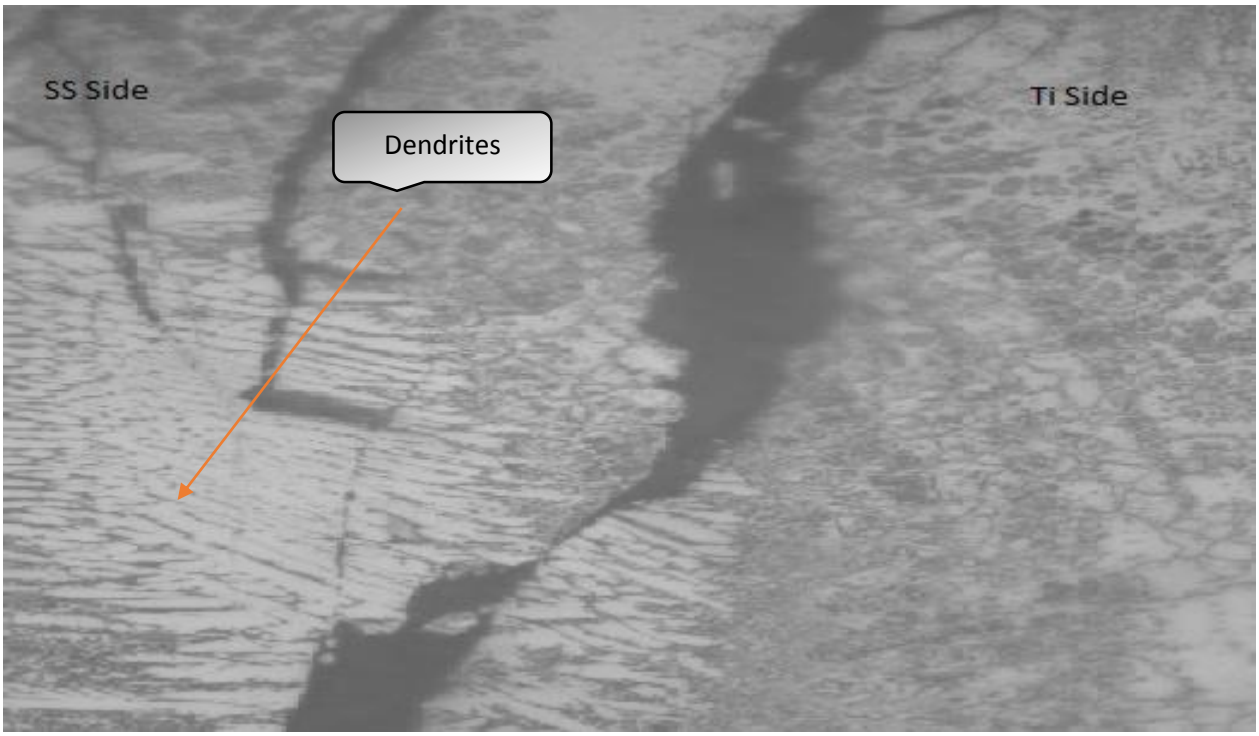

Figure 4.8: Optical Micrograph of SS-Ti at 500x. Note coarse dendritic structure.

The intermetallic compounds couldn't be controlled at such power and speed. The thickness of intermetallic compounds varied a lot along the interface. This variation of thickness along the interface result in spontaneous fracture of the joint right after the weld. This variation of thickness may be due to difference in thermal conductivity between titanium alloy (5.44 W/mK at 20 ^{o}C) and stainless steel (12.1 W/mK, at 20 ^{o}C). Titanium has lower thermal conductivity than stainless

steel which means thermal conduction from lower temperature zone of molten pool is difficult to higher temperature zone. As a result temperature distribution isn't achieved properly that causes uneven distribution of intermetallic compounds along the interface. This uneven distribution of intermetallics has negative impact on the joint's mechanical property. Uneven distribution of intermetallics causes unequal distribution of residual stresses in weld zone. Stress concentration is generated inside the weld zone. These residual stresses become the major cause of cracks initiation at the top of the joint. As mechanical properties of the joint are effected by the variation of intermetallic thickness, this uneven distribution of intermetallics is the major cause of joint failure.

4.4.2 Laser welding of SS 316L and Ti-6Al-4V (With Copper as filler)

The basic purpose of using interlayer in welding is to prevent the irreconcilable materials from mixing. Secondly, to reduce fusion of titanium because it form intermetallic phases with steel and copper elements. The weld between SS-Ti has been cracked spontaneously after welding. Audible cracking was observed during cooling after solidification. Figure 4.9 showed the cross section of the cracked weld. The weld has been broken at multiple places. Multiple throughout cracks and partially grown cracks are visible in the Figure 4.9. The shapes of the cracks suggest that these have been generated due to residual thermal stresses that were produced as a result of uneven heat conduction and uneven distribution of intermetallics.

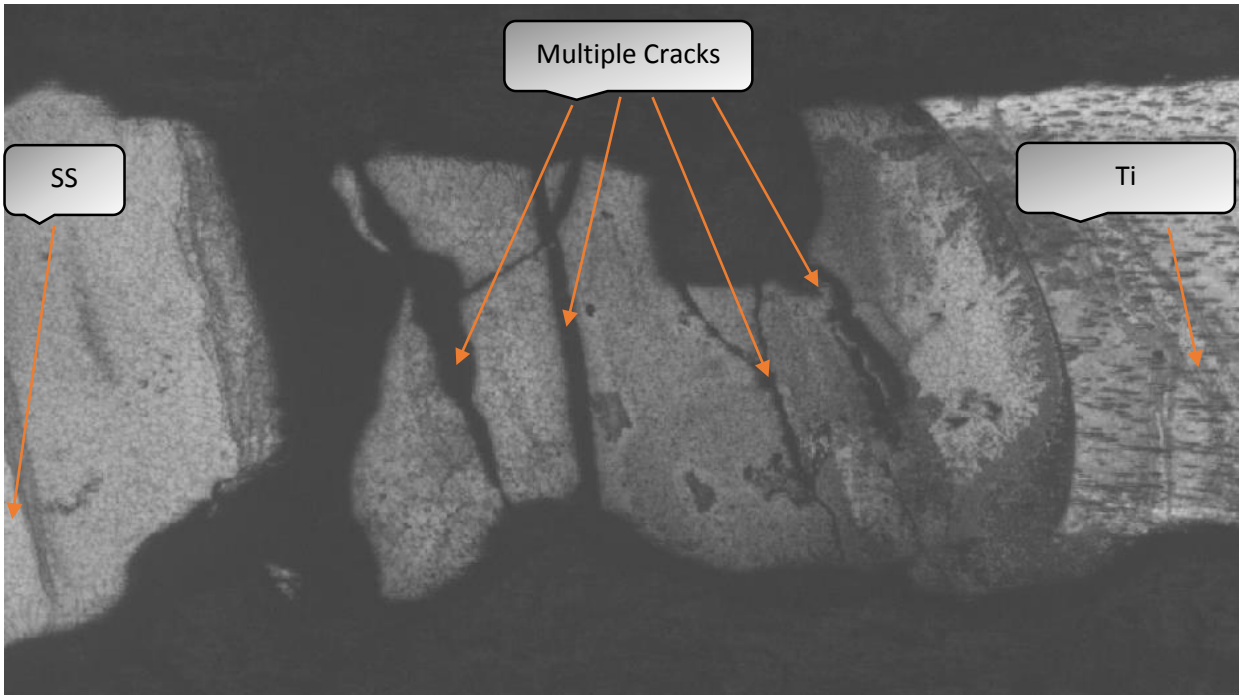

Figure 4.9: Microstructure of SS-Ti pair using Cu as interlayer (50x)

Figure 4.10 (a), (b), (c) and (d) shows optical micrograph of the parent stainless steel (500x), titanium (500x), fusion zone of SS-Ti with copper filler (Ti Side) (200x) and fusion zone of SS-Ti with copper filler (SS side) (200x) respectively.

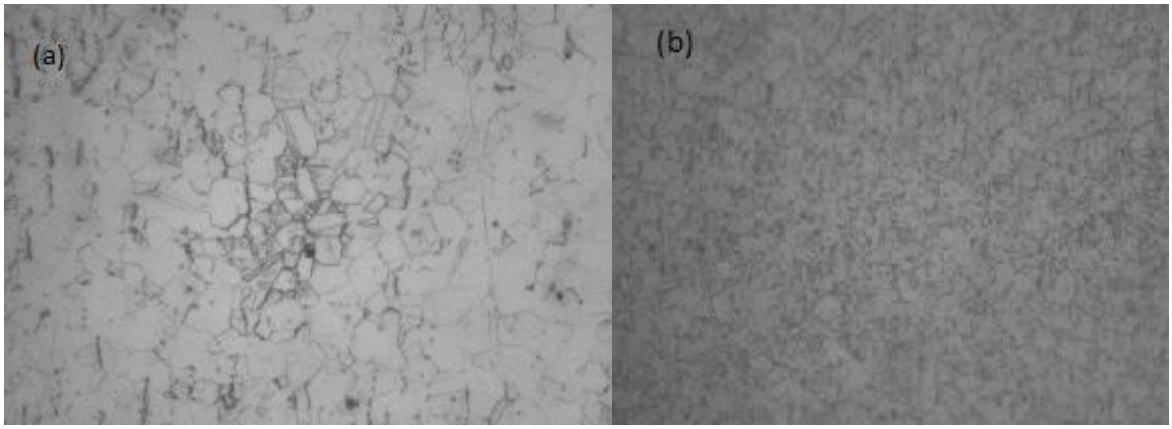

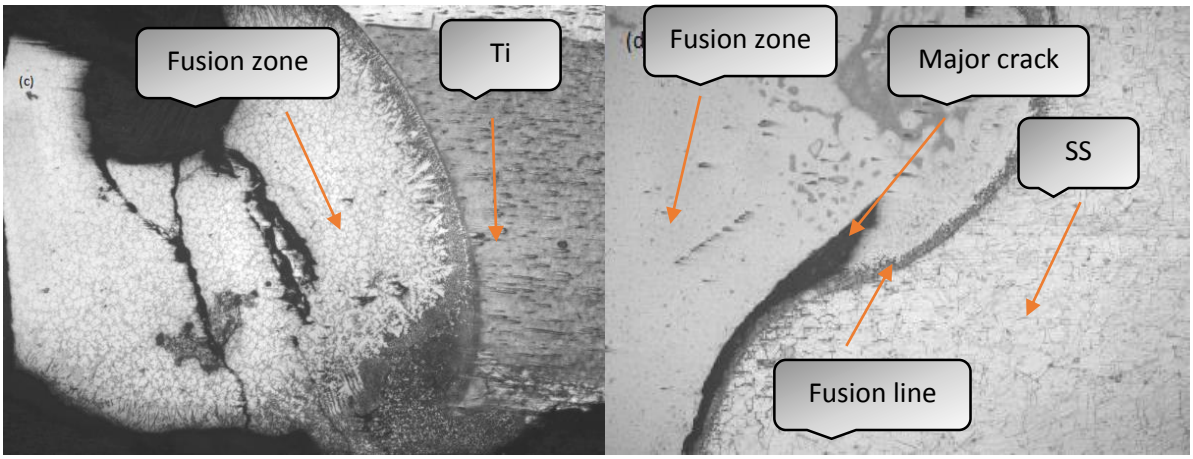

Figure 4.10: (a) Parent Ti metal (b) Parent SS metal (c) HAZ and fusion zone (Ti side) (d) HAZ and fusion zone (SS side)

As filler material is added and due to high cooling speeds, microstructure obtained is extremely complex. Above figures shows microstructures of laser welded joint using copper as filler obtained from optical microscope. Dark areas on the interface of titanium and weld zone are mainly composed of Cu_2Ti phase and some proportion of FeTi phase as shown in Figure 4.10 (c). Weld zone near the stainless steel is mainly composed from solid solution of Ni, Cr and Cu dissolved in iron Fe as shown in Figure 4.10 (d). Complex microstructure obtained is due to rapid solidification process. Titanium has the highest melting temperature of 1665^{o}C, solidification occurs on the interface between molten pool and titanium. After that, melted zone of SS solidify whose melting temperature is 1365^{o}C. According to iron-titanium (Fe-Ti) phase diagram [54], phase formation of Fe_2Ti starts at 1427^{o}C and FeTi phase formation starts at 1317^{o}C. Thirdly and lastly, solidification of copper zone starts. Cu is soluble in Fe up to 4% at 1100^{o}C temperature and diffusion is slowed by rapid cooling resulting increase hardness in welding zone. According to Titanium-Copper phase diagram, Ti_2Cu phase is formed at 1005^{o}C and TiCu phase at 982^{o}C [60].

Figure 4.10 (d) shows a major crack that starts from the mid of interface between fusion line and fusion zone at SS and it penetrates to the end of weld. The basic purpose of using copper as interlayer was to limit the diffusion of Cr and Fe in Ti alloy and also to limit diffusion of titanium in stainless steel. Formation of most brittle phases Cr_2Ti and Fe_2Ti wasn't able to be suppressed resulting in failure of joint [15]. Increasing the thickness of copper filler, increasing power, scan speed and offsetting the laser beam on SS may result in better limiting the brittle intermetallics and achieving in successful joint.

4.4.3 Laser welding of SS 316L and Ti-6Al-4V (Nickel as filler)

Figure 4.11 shows the cross section of the weld. The fusion line at the SS and fusion zone shows complete bonding and no cracks are present. The weld cracked from the titanium side. A single major crack that initiated from the bottom of weld. Result suggests that intermetallics formed at the titanium interface wasn't able to be controlled resulting in fracture. The weld cracked may be due to residual stresses generated due to uneven distribution of intermetallics formed at the titanium interface. Nickel wasn't able to suppress the formation of intermetallics i.e. $FeTi_2$ and FeTi.

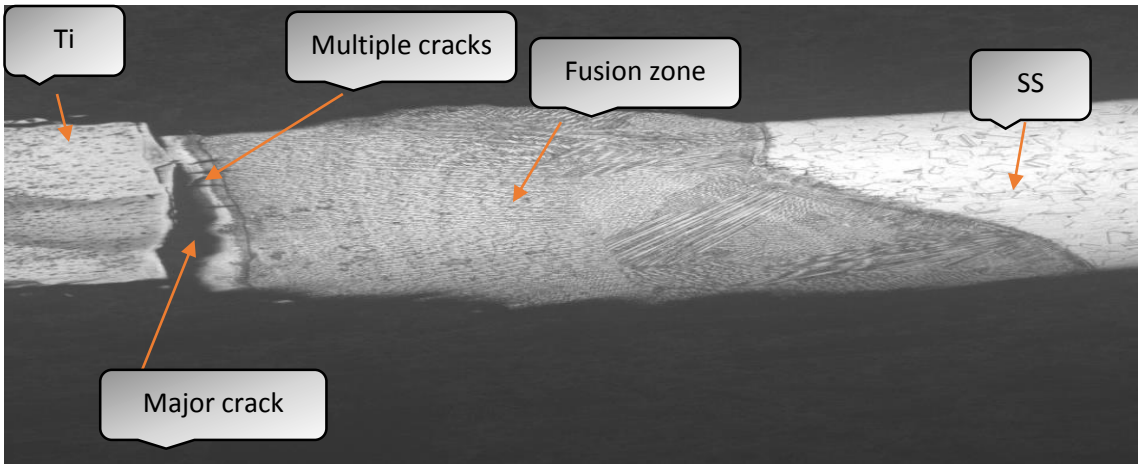

Figure 4.11: Cross-section of the weld using optical microscope (50x)

Figure 4.12 shows the existence of multiple cracks at the interface of titanium base plate and weld zone. These cracks are present perpendicular to the direction of weld zone. Dendrites are observed during the solidification zone are orientated in a specific direction.

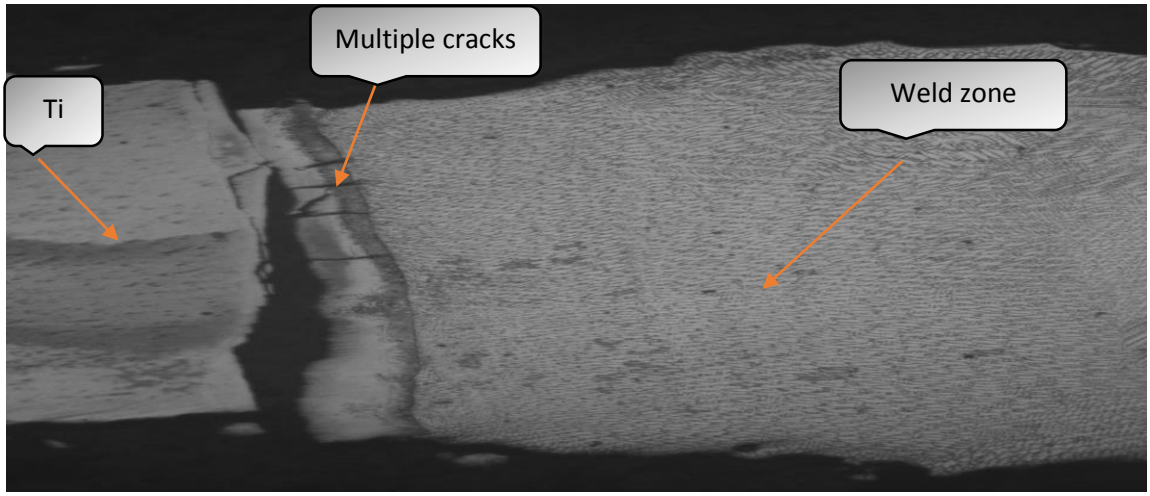

Figure 4.12: Weld cross section taken form Optical Microscope (200x). Note presence of multiple cracks at the interface of titanium and weld zone. Orientated dendrites are also observed in the weld zone.

Figure 4.13 shows the interface between SS and weld zone. No cracking is observed. Dendrites formed are oriented in specific direction.

Figure 4.13: Interface between SS and weld zone.

Increasing laser power, thickness of nickel filler and decreasing the melting of titanium may result in suppressing the intermetallics. Also offsetting the laser to SS may result in suppressing the intermetallics and to achieve successful joint.

4.4.4 Laser welding of SS 316L and Ti-6Al-4V (Aluminium as filler)

Figure 4.14 shows the cross section of weld. Proper penetration wasn't achieved due to high reflectivity of aluminium. Small portion of titanium is melted resulting in fine grain size at the interface. Aluminium due to high reflectivity wasn't able to completely fuse between SS and Ti. Only top surface of the interface between SS and Ti melted properly. Through penetration wasn't achieved as scene clearly in Figure 4.14. Heat affected zone developed on titanium side is shown in Figure 4.15.

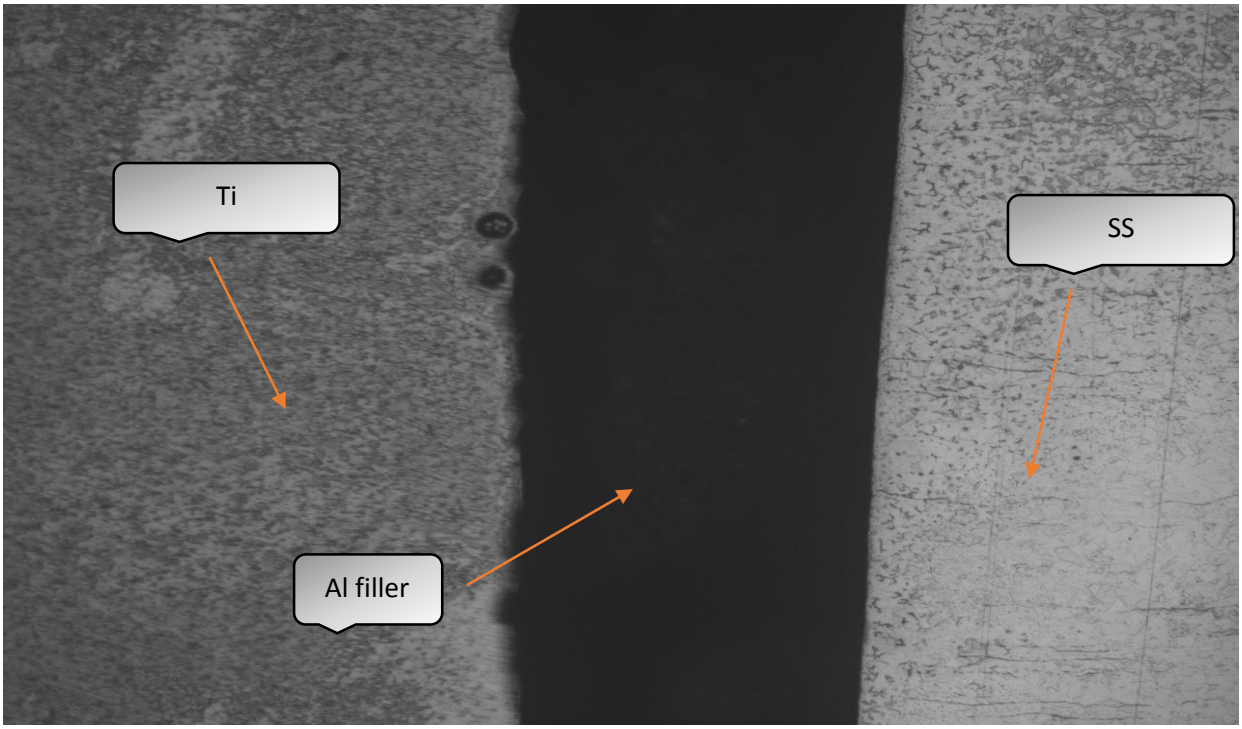

Figure 4.14: Cross section of weld using optical microscope (100x).

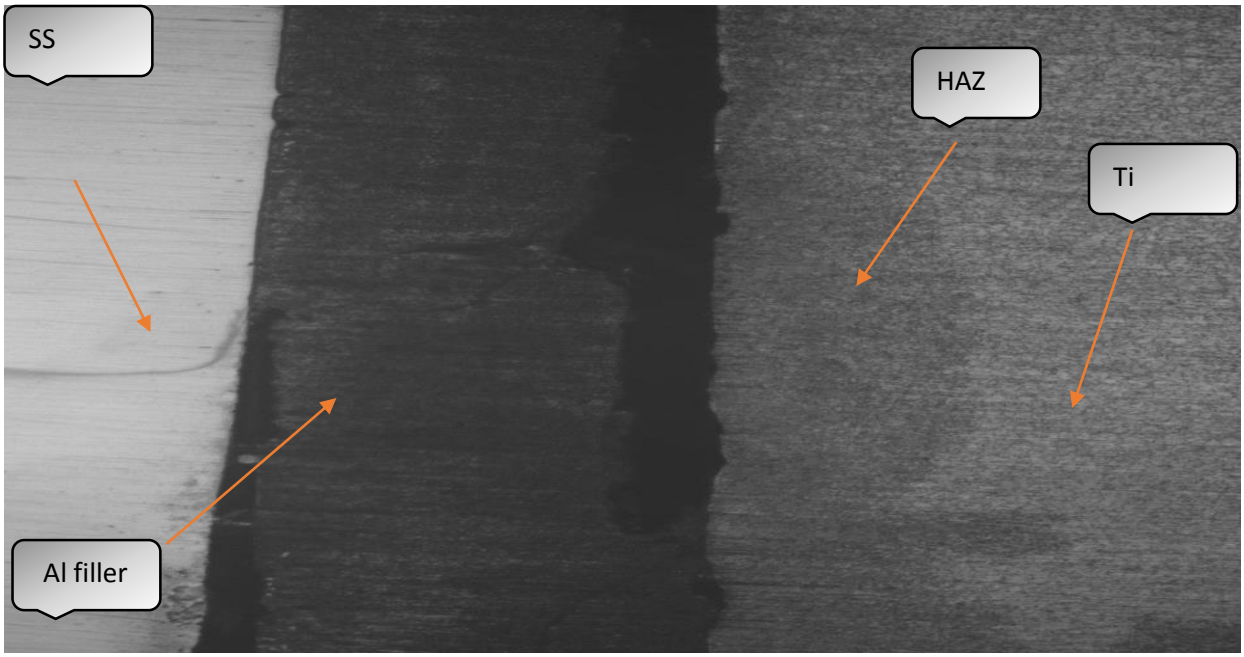

Figure 4.15: Heat affected zone on titanium side.

CO_2 laser isn't preferred when dealing with high reflective material like aluminium. Nd:YAG is preferred for welding purpose when dealing with high reflective materials. Due to unavailability of Nd:YAG laser, CO_2 laser was used for welding. Previously, successful laser welding brazing was done to weld titanium Ti-6Al-4V to aluminium 5A06 [61]. Laser welding with aluminium as filler is possible if Nd:YAG laser is used.

4.5 Micro hardness variation across the welded samples

4.5.1 Micro hardness variation across the laser welded SS-Ti (Without filler)

Hardness variation across the samples has been shown in Table 4.3. Graph is plotted showing the variation of hardness across the weld zone in Figure 4.16.

Table 4.3: Hardness variation across the weld zone.

Sample W3	P (kg)	L (mm)	L^2 (mm^2)	DPH (kg/mm^2)
1	6	0.196	0.038416	289.5668471
2	6	0.19	0.0361	308.1440443
3	6	0.1915	0.036672	303.3356284
4	6	0.135	0.018225	610.3703704
5	6	0.139	0.019321	575.746597
6	6	0.142	0.020164	551.6762547
7	6	0.141	0.019881	559.5291987
8	6	0.1475	0.021756	511.3013502
9	6	0.24	0.0576	193.125
10	6	0.236	0.055696	199.7270899
11	6	0.234	0.054756	203.1558185
12	6	0.23	0.0529	210.2835539

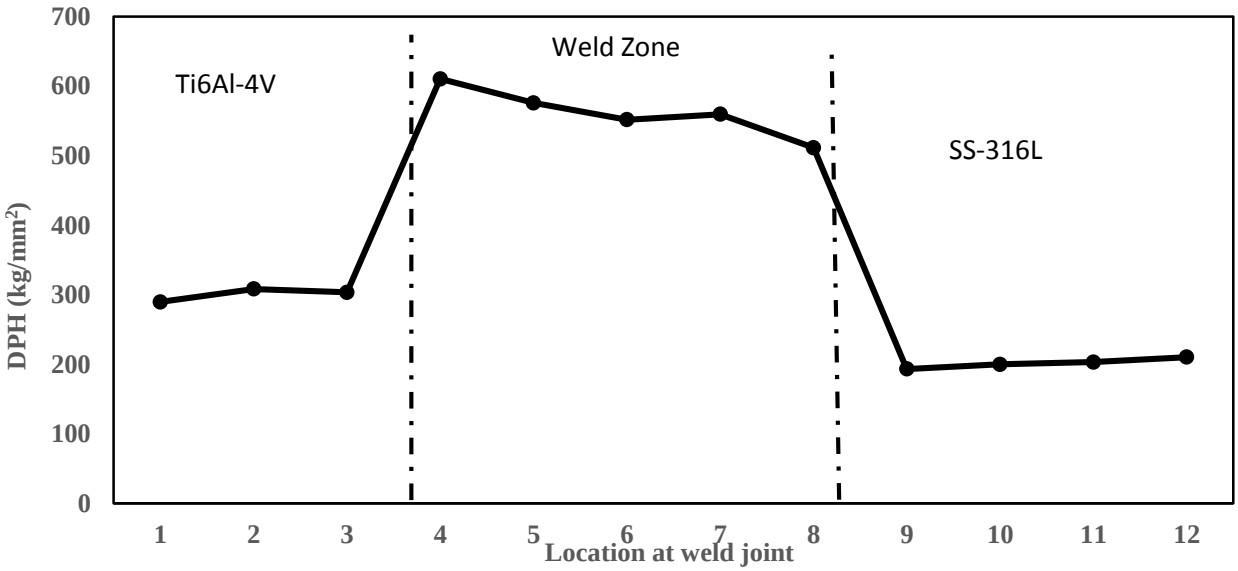

Figure 4.16: Hardness value at different weld zone.

Variation of hardness across the weld describes the localization of brittle intermetallic phases in weld zone. Graph shows that hardness value is considerably higher in weld zone as compared to base metal. The maximum value observed is 559 DPH in weld zone where titanium concentration is maximum. Minimum hardness is in stainless steel that is 210 DPH.

4.5.2 Hardness variation across the laser welded SS-Ti (Copper as filler)

Hardness variation across the samples has been shown in Table 4.4. Graph is plotted showing the variation of hardness across the weld zone in Figure 4.17.

Table 4.4: Hardness variation across the weld zone.

Sample C6.1	P (kg)	L (mm)	L^2 (mm^2)	DPH (kg/mm^2)
1	6	0.196	0.038416	289.5668471
2	6	0.198	0.039204	283.7465565
3	6	0.187	0.034969	318.1103263
4	6	0.138	0.019044	584.120983
5	6	0.141	0.019881	559.5291987
6	6	0.14	0.0196	567.5510204
7	6	0.145	0.021025	529.0844233
8	6	0.142	0.020164	551.6762547
9	6	0.185	0.034225	325.0255661
10	6	0.246	0.060516	183.8191553
11	6	0.24	0.0576	193.125
12	6	0.239	0.057121	194.7444898

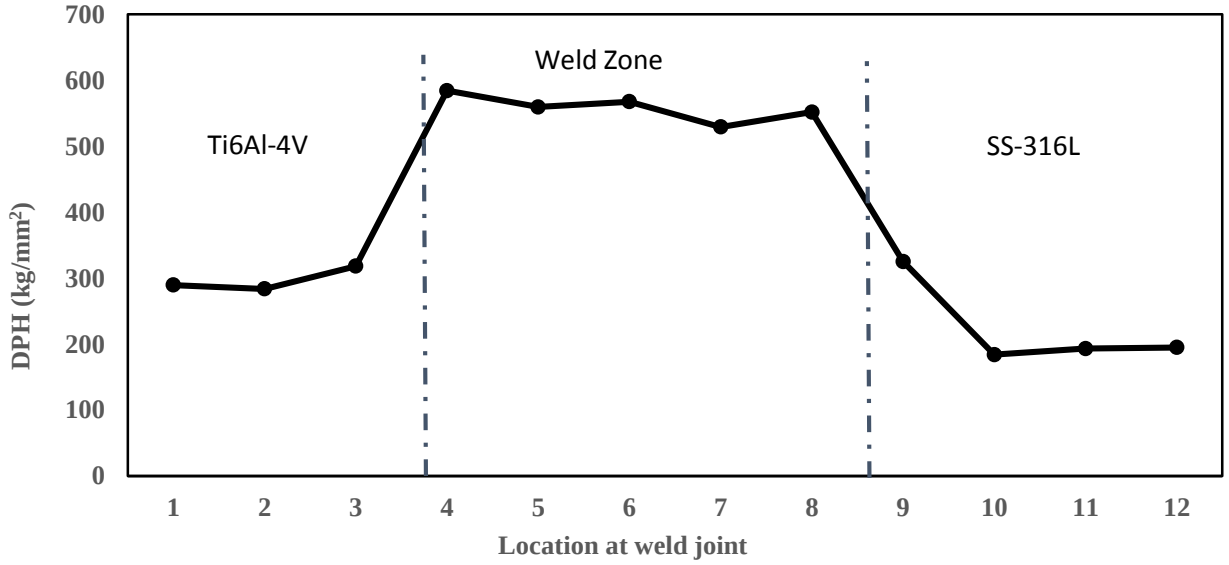

Figure 4.17: Hardness value at different weld zone.

Variation of hardness across the weld describes the localization of brittle intermetallic phases in weld zone. Graph shows that hardness value is considerably higher in weld zone as compared to base metal. The maximum value observed is 584 DPH in weld zone near titanium and weld zone interface where concentration of Ti is maximum. Minimum hardness is in stainless steel that is 194 DPH.

4.5.3 Hardness variation across the laser welded SS-Ti (Nickel)

Hardness variation across the samples has been shown in Table 4.5. Graph is plotted showing the variation of hardness across the weld zone in Figure 4.18.

Table 4.5: Hardness variation across the weld zone.

Sample N1	P (kg)	L (mm)	L^2 (mm^2)	DPH (kg/mm^2)
1	6	0.2	0.04	278.1
2	6	0.1945	0.03783	294.0503962
3	6	0.1945	0.03783	294.0503962
4	6	0.184	0.033856	328.5680529
5	6	0.19	0.0361	308.1440443
6	6	0.175	0.030625	363.2326531
7	6	0.17	0.0289	384.9134948
8	6	0.181	0.032761	339.5500748
9	6	0.24	0.0576	193.125
10	6	0.24	0.0576	193.125
11	6	0.2455	0.06027	184.5686719
12	6	0.2425	0.058806	189.1635668

Figure 4.18: Hardness value at different weld zone.

Graph 4.7 shows that hardness value is considerably higher in weld zone as compared to base metal. The maximum value observed is 384 DPH in weld zone. The value of this hardness as compared to laser welded sample with copper filler and autogenous weld is lower due to addition of nickel as filler. Nickel as filler decreases the hardness in the weld zone. Hardness in stainless steel is found to be 189 DPH.

4.5.4 Hardness variation across the laser welded SS-Ti (Aluminium)

Hardness variation across the samples has been shown in Table 4.6. Graph is plotted showing the variation of hardness across the weld zone in Figure 4.19.

Table 4.6: Hardness variation across the weld zone.

Sample A3.1	P (kg)	L (mm)	L^2 (mm^2)	DPH (kg/mm^2)
1	6	0.19	0.0361	308.1440443
2	6	0.193	0.037249	298.6388896
3	6	0.19375	0.037539	296.3313215

4	6	0.152	0.023104	481.4750693
5	6	0.15	0.0225	494.4
6	6	0.153	0.023409	475.2018454
7	6	0.151	0.022801	487.8733389
9	6	0.16	0.0256	434.53125
10	6	0.24	0.0576	193.125
11	6	0.248	0.061504	180.8662851
12	6	0.24475	0.059903	185.7015716

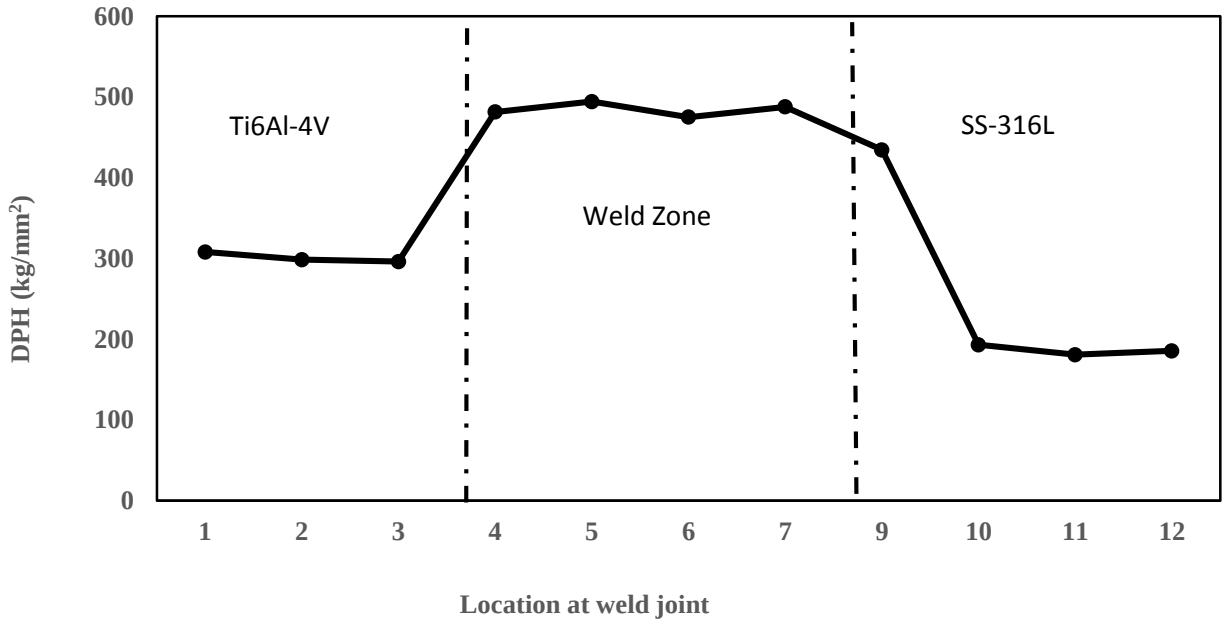

Figure 4.19: Hardness value at different weld zone.

Figure 4.19 illustrates hardness to be higher in weld zone. The hardness in weld zone is comparable to hardness in autogenous welding and welding with copper as filler. The maximum value obtained in hardness is observed to be 487 DPH in weld zone. Minimum hardness is observed to be in base plate of SS that is 180 DPH.

Chapter 5

Future Work and Concluding Remarks

5.1 Conclusion

Based on experimental results and discussion, following conclusion were drawn.

1. Hardness across the beads on plate weld was performed for SS and Ti. Hardness value showed to be maximum in welding zone for titanium and in SS it is observed to be maximum in heat affected zone.
2. Decreasing the scan speed at constant power has minor effect on hardness in both SS and Ti beads on plate weld samples.
3. Hardness across the weld zones of SS-Ti (with and without filler) showed increase hardness in the weld zone as compared to base metals.
4. The width and depth of weld zone decreases with increase in speed for laser operating at constant power. This is due to lower thermal input at higher speeds.
5. Lase welding was performed at low power of 650W and scan speed of 300 mm/min. Majority of weld cracked from the titanium side. Cracks were due to uneven distribution of intermetallics along the weld zone and due to formation of brittle intermetallics. Filler materials added wasn't able to suppress the formation of brittle intermetallics due to low power and scan speed. Laser beam was offset on Ti, which helped in melting the Ti as it has higher melting point but due to lower thermal conductivity, uneven distribution of intermetallics was observed which is the main cause of failure of joint.

6. Increasing the laser power, scan speed, thickness of fillers and offsetting the laser on SS side can result in durable joint.

References

1. Szymanski, Z., J. Kurzyna, and W. Kalita, *The spectroscopy of the plasma plume induced during laser welding of stainless steel and titanium.* Journal of Physics D: Applied Physics, 1997. **30**(22): p. 3153.
2. Mai, T. and A. Spowage, *Characterisation of dissimilar joints in laser welding of steel–kovar, copper–steel and copper–aluminium.* Materials Science and Engineering: A, 2004. **374**(1): p. 224-233.
3. Borrisutthekul, R., Y. Miyashita, and Y. Mutoh, *Dissimilar material laser welding between magnesium alloy AZ31B and aluminum alloy A5052-O.* Science and Technology of Advanced Materials, 2005. **6**(2): p. 199-204.
4. Ghosh, M., S. Chatterjee, and B. Mishra, *The effect of intermetallics on the strength properties of diffusion bonds formed between Ti–5.5 Al–2.4 V and 304 stainless steel.* Materials Science and Engineering: A, 2003. **363**(1): p. 268-274.
5. Akbari Mousavi, S. and P.F. Sartangi, *Effect of post-weld heat treatment on the interface microstructure of explosively welded titanium–stainless steel composite.* Materials Science and Engineering: A, 2008. **494**(1): p. 329-336.
6. Kundu, S., et al., *Influence of interface microstructure on the mechanical properties of titanium/17-4 PH stainless steel solid state diffusion bonded joints.* Materials & Design, 2012. **37**: p. 560-568.
7. Kundu, S., S. Sam, and S. Chatterjee, *Interface microstructure and strength properties of Ti–6Al–4V and microduplex stainless steel diffusion bonded joints.* Materials & Design, 2011. **32**(5): p. 2997-3003.
8. Akbari Mousavi, S. and P. Farhadi Sartangi, *Experimental investigation of explosive welding of cp-titanium/AISI 304 stainless steel.* Materials & Design, 2009. **30**(3): p. 459-468.
9. Song, J., et al., *Hierarchical microstructure of explosive joints: Example of titanium to steel cladding.* Materials Science and Engineering: A, 2011. **528**(6): p. 2641-2647.
10. Yue, X., et al., *Microstructure and interfacial reactions of vacuum brazing titanium alloy to stainless steel using an AgCuTi filler metal.* Materials Characterization, 2008. **59**(12): p. 1721-1727.
11. Lee, M.K., et al., *Formation of interfacial brittle phases sigma phase and IMC in hybrid titanium-to-stainless steel joint.* Transactions of Nonferrous Metals Society of China, 2011. **21**: p. s7-s11.
12. Chen, S., et al., *Microstructures and mechanical property of laser butt welding of titanium alloy to stainless steel.* Materials & Design, 2014. **53**: p. 504-511.
13. Satoh, G., Y.L. Yao, and C. Qiu, *Strength and microstructure of laser fusion-welded Ti–SS dissimilar material pair.* The International Journal of Advanced Manufacturing Technology, 2013. **66**(1-4): p. 469-479.
14. Williams, D.F., *Biocompatibility of clinical implant materials*. Vol. 1. 1981: CRC press Boca Raton, Florida.
15. Tomashchuk, I., et al., *The formation of intermetallics in dissimilar Ti6Al4V/copper/AISI 316 L electron beam and Nd: YAG laser joints.* Intermetallics, 2011. **19**(10): p. 1466-1473.
16. O'shea, D.C., et al., *AnIntroductiontoLasersandTheirApplications.* American Journal of Physics, 1978. **46**(5): p. 592-592.

17. BEESLEY, M., *Lasers and their applications(Book on lasers and applications covering theories of light, polarization, coherence, resonators, mirrors, modes, electro-optical effect, communication, holography, etc).* London, Taylor and Francis, Ltd., 1971. 243 p, 1971.
18. Migliore, L.R., *Laser materials processing*1996: CRC Press.
19. Duley, W.W., *CO2 lasers: Effects and applications.* NASA STI/Recon Technical Report A, 1976. **77**: p. 15811.
20. Baardsen, E., D. Schmatz, and R. Bisaro, *High speed welding of sheet steel with a CO 2 laser.* Welding Journal, 1973. **52**: p. 227-229.
21. Locke, E., E.D. Hoag, and R. Hella, *Deep penetration welding with high-power CO 2 lasers.* Quantum Electronics, IEEE Journal of, 1972. **8**(2): p. 132-135.
22. Willgoss, R., J. Megaw, and J. Clark, *ASSESSING THE LASER FOR POWER-PLANT WELDING.* Welding and Metal Fabrication, 1979. **47**(2): p. 117-&.
23. Harry, J.E., *Industrial lasers and their applications.* NASA STI/Recon Technical Report A, 1974. **75**: p. 15322.
24. Steen, W., *Surface engineering with lasers*1987: Springer.
25. Roessler, D.M., *An introduction to the laser processing of materials*. Vol. 629. 1986: SPIE.
26. Ready, J., *Effects of High Power Laser Radiation (Academic, New York, 1971).* Chap. **3**: p. 18.
27. Seaman, F., *The Role of Focus in Heavy-Plate Laser Welding.* SME Technical Paper MR78-345, Society of Manufacturing Engineers, Dearborn, Michigan, 1978.
28. Engel, S.L., *Kilowatt welding with a laser.* Laser Focus, 1976. **12**: p. 44-47.
29. Alexender, J., 1982, University of London.
30. Banas, C.M., *High power laser welding-1978.* Optical Engineering, 1978. **17**(3): p. 173210-173210-.
31. Eboo, G.M., 1979, University of London.
32. Arata, Y. and I. Miyamoto, *Laser welding.* Technocrat, 1978. **11**(5): p. 33-42.
33. Merchant, V., M. Cervenan, and H. Seguin, *New Developments in High Power Laser Welding.* Welding for Challenging Environments, 1985: p. 31-40.
34. Seaman, F., *The Role of Shielding Gas in High Power CO 2 (CW) Laser Welding.* Technical Paper MR77-982, Society of Manufacturing Engineers, Dearborn, MI, 1977.
35. Herziger, G., E.W. Kreutz, and K. Wissenbach. *Fundamentals of laser processing of materials*. in *1986 Quebec Symposium*. 1986. International Society for Optics and Photonics.
36. Sun, Z. and R. Karppi, *The application of electron beam welding for the joining of dissimilar metals: an overview.* Journal of Materials Processing Technology, 1996. **59**(3): p. 257-267.
37. Li, Z. and G. Fontana, *Autogenous laser welding of stainless steel to free-cutting steel for the manufacture of hydraulic valves.* Journal of Materials Processing Technology, 1998. **74**(1): p. 174-182.
38. Orhan, N., M. Aksoy, and M. Eroglu, *A new model for diffusion bonding and its application to duplex alloys.* Materials Science and Engineering: A, 1999. **271**(1): p. 458-468.
39. Béjar, M., W. Schnake, and R. Urqueta, *Electrocontact-discharge forge welding of steel bars.* Journal of Materials Processing Technology, 2002. **127**(1): p. 68-72.

40. Kaçar, R. and O. Baylan, *An investigation of microstructure/property relationships in dissimilar welds between martensitic and austenitic stainless steels.* Materials & Design, 2004. **25**(4): p. 317-329.
41. Satyanarayana, V., G. Madhusudhan Reddy, and T. Mohandas, *Dissimilar metal friction welding of austenitic–ferritic stainless steels.* Journal of Materials Processing Technology, 2005. **160**(2): p. 128-137.
42. Srinivasan, P.B., et al., *An assessment of impact strength and corrosion behaviour of shielded metal arc welded dissimilar weldments between UNS 31803 and IS 2062 steels.* Materials & Design, 2006. **27**(3): p. 182-191.
43. Berretta, J.R., et al., *Pulsed Nd: YAG laser welding of AISI 304 to AISI 420 stainless steels.* Optics and Lasers in Engineering, 2007. **45**(9): p. 960-966.
44. Luijendijk, T., *Welding of dissimilar aluminium alloys.* Journal of Materials Processing Technology, 2000. **103**(1): p. 29-35.
45. Lee, W.-B., Y.-M. Yeon, and S.-B. Jung, *The joint properties of dissimilar formed Al alloys by friction stir welding according to the fixed location of materials.* Scripta Materialia, 2003. **49**(5): p. 423-428.
46. Zhang, H., et al., *Interfacial microstructure and strength of the dissimilar joint Ti< sub> 3</sub> Al/TC4 welded by the electron beam process.* Materials Science and Engineering: A, 2006. **425**(1): p. 255-259.
47. Abdollah-Zadeh, A., T. Saeid, and B. Sazgari, *Microstructural and mechanical properties of friction stir welded aluminum/copper lap joints.* Journal of Alloys and Compounds, 2008. **460**(1): p. 535-538.
48. Zumelzu, E. and C. Cabezas, *Study on welding such dissimilar materials as AISI 304 stainless steel and DHP copper in a sea-water environment. Influence of weld metals on corrosion.* Journal of Materials Processing Technology, 1996. **57**(3): p. 249-252.
49. Sahin, A.Z., et al., *Analysis of the friction welding process in relation to the welding of copper and steel bars.* Journal of Materials Processing Technology, 1998. **82**(1): p. 127-136.
50. Mathieu, A., et al., *Dissimilar material joining using laser (aluminum to steel using zinc-based filler wire).* Optics & Laser Technology, 2007. **39**(3): p. 652-661.
51. Liu X. Pang M, Z.C., Fan J., *Dissimilar autogenous full penetration welding of super-alloy K418 and 42CrMo steel by a high power CW Nd:YAG laser,.* Journal of Applied Surface Science, 2007. **253**(17).
52. Ventrella, V.A., J.R. Berretta, and W. De Rossi, *Pulsed Nd: YAG laser seam welding of AISI 316L stainless steel thin foils.* Journal of Materials Processing Technology, 2010. **210**(14): p. 1838-1843.
53. Joseph, B., et al., *Weld metal characterization of 316L (N) austenitic stainless steel by electron beam welding process.* International Journal of Engineering, Science and Technology, 2012. **4**(2): p. 169-176.
54. Raghavan, V., G.V. Raynor, and V.G. Rivlin, *Phase diagrams of ternary iron alloys*1987: Indian Institute of Metals.
55. Yu, C., M. Wu, and H. Lu, *Factors influencing formation and growth of coarse Ti–Fe compound in Ti–Fe eutectic reaction.* Science and Technology of Welding & Joining, 2006. **11**(3): p. 265-270.
56. Louzguine-Luzgin, D.V., et al. *Non-equilibrium Ti-Fe bulk alloys with ultra-high strength and enhanced ductility*. in *MRS Proceedings*. 2004. Cambridge Univ Press.

57. Ray, R., B. Giessen, and N. Grant, *The constitution of metastable titanium-rich Ti-Fe alloys: An order-disorder transition.* Metallurgical Transactions, 1972. **3**(3): p. 627-629.
58. Flemings, M.C., *Solidification processing.* Metallurgical Transactions, 1974. **5**(10): p. 2121-2134.
59. David, S., S. Babu, and J. Vitek, *Welding: Solidification and microstructure.* JOM, 2003. **55**(6): p. 14-20.
60. GROZA, C., et al. *Melted zone morphology by laser welding of Ti-6Al-4V with X5CrNi18-10*. in *21nd International Conference on Metallurgy and Materials. Brno, Czech Republic*. 2012.
61. Chen, Y., S. Chen, and L. Li, *Influence of interfacial reaction layer morphologies on crack initiation and propagation in Ti/Al joint by laser welding–brazing.* Materials & Design, 2010. **31**(1): p. 227-233.